

Beryllium Abundances in Stars of One-Solar-Mass

Ann Merchant Boesgaard¹

*Institute for Astronomy, University of Hawai'i at Manoa,
2680 Woodlawn Drive, Honolulu, HI 96822*

boes@ifa.hawaii.edu

Julie A. Krugler¹

*Department of Physics & Astronomy,
Michigan State University, East Lansing, MI 48824-1116*

kruglerj@msu.edu

ABSTRACT

We have determined Be abundances in 50 F and G dwarfs in the mass range of $0.9 \leq M_{\odot} \leq 1.1$ as determined by Lambert & Reddy. The effective temperatures are 5600 to 6400 K and metallicities from -0.65 to $+0.11$. The spectra were taken primarily with Keck I + HIRES. The Be abundances were found via spectral synthesis of Be II lines near 3130 Å. The Be abundances were investigated as a function of age, temperature, metallicity and Li abundance in this narrow mass range. Even though our stars are similar in mass, they show a range in Be abundances of a factor of >40 . We find that $[\text{Be}/\text{Fe}]$ has no dependence on temperature, but does show a spread of a factor of 6 at a given temperature. The reality of the spread is shown by two identical stars which differ from each other by a factor of two only in their abundances of Li and Be. Our thin-disk-star sample fits the trend between Be abundance and $[\text{Fe}/\text{H}]$ found for halo and thick disk stars, extending it to about 4 orders of magnitude in the two logarithmic quantities. Both Fe and Be appear to increase similarly over time in the Galaxy. One-third of our sample may be classified as subgiants; these more-evolved stars have lower Be abundances than the dwarfs. They have undergone Be depletion by slow mixing on the main sequence and Be dilution during their trip toward the red giant base. There are both Li and Be detections in 60 field stars in the

¹Visiting Astronomer, W. M. Keck Observatory jointly operated by the California Institute of Technology and the University of California.

“Li-plateau” of 5900 - 6300 K now and the abundances of the two light elements are correlated with a slope of 0.34 ± 0.05 , with greater Li depletion than Be depletion.

Subject headings: stars: Abundances; stars: solar-type; stars: evolution; stars: late-type; stars: Population I

1. INTRODUCTION

The study of the light elements reveals the physics of a star beneath its surface. Lithium, Be, and B can all be used as probes to understand surface mixing down to temperatures of about 2.5×10^6 , 3.5×10^6 , and 5×10^6 K respectively, where they are destroyed by fusion primarily with protons. Boron provides the deepest look into the interior of a star, but the B I, B II, and B III resonance lines appear only in the “satellite” UV so it is impossible to find B abundances without going above the atmosphere. Lithium is markedly easier to observe given that its resonance doublet occurs in the red portion of the spectrum at 6708 Å, but inasmuch as there are multiple sites for the creation and destruction of Li, the interpretation of the Li abundance can be complicated. Beryllium provides a clearer picture as it has one mechanism of production: spallation reactions in the vicinity of supernovae or in the ambient interstellar gas. The resonance lines of Be II are found at 3130.421 and 3131.065 Å, which are still observable with ground-based telescopes. However, the Be II features are near the atmospheric cutoff (~ 3000 Å), so stars must be observed at low air mass.

There have been several recent studies of the light elements Li and Be. Boesgaard et al. (2004a) (hereinafter B04a) investigated the correlation of Li and Be in F and G dwarf stars in cluster and field stars in the metallicity range of $-0.45 \leq [\text{Fe}/\text{H}] \leq +0.11$. Included in the paper was a plot of the Be abundance against T_{eff} from a variety of cluster and field sources. The plot showed a large spread in $A(\text{Be}) = \log N(\text{Be})/N(\text{H}) + 12.00$ and the focus of their study was narrowed by defining two temperature regimes: the cool side of the Li-Be dip (Boesgaard & Tripicco 1986; Boesgaard & King 2002) from 6300-6650 K (where Li increases with decreasing temperature) and near the Li plateau from 5900-6300 K (where Li begins to decline with decreasing temperature). B04a found that Li was depleted more than Be in both temperature regimes. The amount of Li and Be depletion in the Li-Be dip ($T_{\text{eff}} = 6300 - 6650$ K) is attributed to slow mixing and is dependent upon age and temperature. Older stars showed more Li and Be depletion and the hotter stars, near the bottom of the dip, show the greatest depletions. There was no difference in the depletion patterns between the cluster and field stars.

Santos et al. (2004a) (hereafter S04a) determined Be abundances by spectrum synthesis in field stars ranging from 4800-6300 K. They found the Be abundance to peak at ~ 6100 K, with decreasing Be abundances both towards the cooler stars and towards the Li-Be gap that encompasses hotter stars. They suggest that the peak may be explained by a the bias in their sample of metal-rich stars which would also have enhanced Be due to Galactic enrichment. They discuss the decline in the Be abundance and the possibility of a Be plateau around $T_{\text{eff}} \sim 5600$ K. This decline and plateau are compared to the Be depletion models that introduce rotational mixing by Pinsonneault et al. (1990) for 1.7 Gyr ages. The match is acceptable above 5600 K, but there is a better fit for cooler temperatures with the wave-driven mixing models of 4.5 Gyr of Montalbán & Schatzman (2000). This same data set was also analyzed in Santos et al. (2004b) to find a possible correlation between Be abundance and planet hosts. It was found that planet hosts have a “normal” Be abundance.

Lambert & Reddy (2004; hereafter LR04) have compiled a database of Li abundances for 451 F and G thin disc stars. The stars were taken from three different surveys of Li in field stars: Reddy et al. (2003), Chen et al. (2001), and Balachandran (1990). The stars are located in the solar neighborhood and have measured Hipparcos parallaxes. HR diagrams were created for these field stars using the parallaxes to calculate M_V . The majority of these stars were slightly evolved away from the zero age main sequence, so it was possible to calculate evolutionary ages from the Girardi et al. (2000) (hereafter G00) isochrones. The corresponding evolutionary tracks were used to determine masses for each metallicity subset.

It has been shown to be useful to study more than one of the light elements at once to develop a fuller picture of the stellar mixing and depletion processes. For example, B04a investigate the correlation of Li and Be, and Boesgaard et al. (2005) discovered the correlation of Be and B.

The location of the Li resonance lines in the red spectral region makes Li easier to observe and measure than Be, due to the location of the Be II lines near the atmospheric cut off and due to the substantial blending found in the UV in solar-type stars. Given that the LR04 data have a complete set of stellar parameters, along with Li abundances, they provide a good base from which to study the Be abundances. In order to disentangle information regarding the Be and Li abundances from the large spread in the B04a plots of $A(\text{Be})$ vs. T_{eff} and $A(\text{Be})$ vs. $[\text{Fe}/\text{H}]$, we placed a one solar mass constraint on the LR04 data in our star selection. In this way we can understand better the nature of the processes which affect both Li and Be at $1 M_{\odot}$.

2. OBSERVATIONS

A total of 52 high resolution spectra of the Be II resonance lines at 3130.421 and 3131.065 Å were taken over several nights with the HIRES instrument on the Keck I 10m telescope and the coudé spectrograph on the Canada-France-Hawaii 3.6m telescope (CFHT). These telescopes are on Mauna Kea at 14,000 feet elevation which is above $\sim 40\%$ of the Earth's atmosphere. This allows additional throughput in the ultraviolet region compared to other observatory sites. Additionally, these spectra were taken when the stars were near the meridian, reducing the air mass and reducing the effects of atmospheric dispersion.

2.1. Star Selection

The stars in this study were chosen from the LR04 paper in which 451 F and G dwarfs were analyzed for the purpose of understanding the metallicity, mass, and age effects on the Li abundance. Their study determined ages and masses using the G00 tracks, and Hipparcos parallaxes for M_V . Our study focused on the stars that LR04 found to be within $0.9 \leq M_{\odot} \leq 1.1$. Of the 451 stars in the LR04 study there were 156, or 35% in that mass range; we have Be observations of one third of these stars.

Figure 1 is an HR Diagram showing the positions of our stars. They are separated into dwarfs and subgiants by the criterion of S04 at $\log g = 4.1$. The circled dot indicates the Sun. They range from $5600 < T_{\text{eff}} < 6600$ and most are somewhat evolved away from the zero age main sequence. Due to the fact that most of the stars in LR04 are evolved beyond the zero age main sequence, it was possible for them to determine stellar ages.

2.2. New Keck/HIRES Observations

In 2004, the HIRES spectrometer was upgraded with a 6144 x 4096 mosaic CCD, which is split into three chips with one optimized for the ultraviolet/blue end of the spectrum. The quantum efficiency is 94% for this chip in the beryllium region, about 12 times better than the old chip. Between 31 January 2005 and 9 June 2007, 40 Keck spectra were taken with the new HIRES detector on nine separate nights. Given the relative brightness of these stars, they were taken in evening and morning twilights and on partly cloudy nights. The decker used was B5 which has slit dimensions of 3.5 x 0.861 arcsec. These data have a spectral dispersion of $0.0132 \text{ \AA pixel}^{-1}$ and a measured spectral resolution of $\sim 49,000$ near 3130 Å. Exposure times ranged from 3-30 minutes to attain a signal-to-noise ratio (S/N) range from 33 to 277 and a median S/N of 146 and a mean of 168.

On each of the nine nights on which observations were made for this program, calibration frames were also taken. Typically 7-9 bias frames were recorded and Th-Ar spectra were obtained at the beginning and end of each night. The internal flat fields were taken with different exposure times for each of the three CCDs. In order to achieve sufficient flux for the Be II line region exposures of 50 s were needed for the UV chip. The optimum exposure for the green chip was typically 3 s and that exposure would be useful for the longer orders of the UV chip. In order not to saturate the flat fields on the red chip exposures of 1 s were obtained. Seven to nine flat exposures were taken at each of the three exposure times to achieve the proper flux for the various orders on all three CCDs.

Table 1 gives the star name, V magnitude, date of observation, exposure time, and total S/N of the stars for which observations were taken using Keck I with the upgraded HIRES.

2.3. Other Observations

The Keck spectra from the upgraded HIRES were supplemented by spectra in the LR04 one-solar-mass range from the original HIRES and the CFHT. With the original HIRES on Keck I with a Tektronix 2048 x 2048 CCD (Vogt et al. 1992), five stars were observed between 13 November 1999 and 5 January 2002. These data have a spectral resolution of $0.022 \text{ \AA pixel}^{-1}$ which gives a resolution of $\sim 48,000$ per pixel. Exposure times for those stars ranged from 5-12 minutes with a median S/N of 140 and a mean of 122.

Five stars were observed on 15 and 16 October 1995 on the 3.6m CFHT with the Gecko f/4 spectrograph with a resolution of $\sim 120,000$ and a dispersion of $0.010 \text{ \AA pixel}^{-1}$. The detector was a 2048 x 2048 array with $15 \mu\text{m}$ pixels that is UV sensitive with a quantum efficiency 80% in the beryllium region. Exposure times for these five stars range from 15-45 minutes, with a median and mean S/N of 72. Information on these observations and data reduction can be found in Boesgaard et al. (2001). One additional star (HD 142860) was obtained with the f/8 coudé spectrograph at CFHT at a resolution of 24,000. Details of that observation can be found in Boesgaard et al. (2004b).

Table 2 includes the CFHT stars and Keck I stars that were previously included in Boesgaard et al. (2001, 2004a, 2004b). It lists the name, V magnitude, date of observation, exposure time, total S/N, telescope, and the reference to the paper from which the star was taken and where the earlier analyses were presented. The Be abundances for these stars have been redetermined here using the parameters determined by LR04.

2.4. Data Reduction

The Keck I data from the upgraded HIRES were reduced using IRAF and using two different reduction pipelines: the new MAKEE Data Reduction Software and the IDL-based HIRES Redux software. Both software routines were designed for the new chip. We used our own master flat fields (one for each chip), biases, and arcs rather than adopt archival ones. It is critical to have long flat field exposures, typically 50 s, in order to have sufficient flux at the UV wavelengths of the Be II lines, while 3 s is enough for the green chip and 1 s for the red chip. Our wavelength calibrations were found from our Th-Ar exposures at the beginning and end of the each night. The wavelength solution was applied for the each night. Cosmic ray removal was also performed on the stars in the Be region using the IDL version of L.A. Cosmic¹. The data were then doppler corrected and continuum fit in IRAF using the onedspec package and the echelle package.

The data reduction for the stars discussed in §2.3 has been described in the original papers; see Boesgaard et al. 2001, B04a, and B04b for the details of the procedures used regarding the CFHT stars and the earlier Keck I HIRES stars.

3. ABUNDANCES

3.1. Stellar Parameters

In order to measure the Be abundance in these stars, we interpolated atmospheric models from the Kurucz grid point models (Kurucz 1993). These require metallicity ($[Fe/H]$), effective temperature (T_{eff}), surface gravity ($\log g$), and microturbulence (ξ). The $[Fe/H]$, T_{eff} , and $\log g$ were adopted from LR04; however, the microturbulence parameter was not included. Microturbulences were determined using the following relation derived by Edvardsson et al. (1993):

$$\xi = 1.25 + 8 \times 10^{-4}(T_{\text{eff}} - 6000) - 1.3(\log g - 4.5)$$

A complete list of the stellar parameters (T_{eff} , $\log g$, $[Fe/H]$, and ξ) for all our stars is found in Table 3.

¹<http://www.astro.yale.edu/dokkum/lacosmic>

3.2. Beryllium Synthesis

We determined the abundance of Be by fitting the Be II resonance lines at 3130.421 and 3131.065 Å using the spectral synthesis software MOOG² (Snedden 1973) as updated in 2002 (in “synth” mode). Due to the considerable blending around the 3130.421 Å line the stronger of the doublet, the fit of the 3131.065 Å line gave a more reliably-determined Be abundance.

Our line list includes 307 atomic and molecular lines between 3129.5 and 3132.5 Å. It was adopted largely from Kurucz to best fit the Be region with some modifications to the list from former studies of Be abundances in stars covering a wide range of temperatures and gravities., e.g. the log gf value of the 3129.763 Å Zr II line. During the synthesis-fitting a Gaussian profile was used for the instrumental and other broadening. The instrumental broadening has a full-width half-maximum of 0.08 Å and most of the stars were fit with FWHM 0.08 to 0.10 Å. The largest broadening was 0.18 Å for HD 218470, an F5 V star in the Li-Be dip region with $T_{\text{eff}} = 6495$ K.

Figures 2-5 show examples of the synthetic spectra that were created for each star. For each spectrum, the dots represent the data points, while the solid line is the synthesis with the best fit. The dash-dotted lines represent a factor of two in the Be abundance above and below the best-fit Be abundance and the dotted line represents a synthetic spectrum without any Be. The Be abundance is represented in terms of $A(\text{Be})$; the meteoritic value is $A(\text{Be})=1.42$ (Grevesse & Sauval 1998).

In Figure 2 HD 693 and HD 103799 are compared. They have essentially the same T_{eff} , $[\text{Fe}/\text{H}]$, age (6.1 Gyr), and $A(\text{Be})$. The main discernible difference is in the rotation as is seen in the line broadening in HD 103799 where its full-width half-maximum (FWHM) gaussian is 0.13 compared to that of HD 693 at 0.09. Shown in Figure 3 are HD 186379 and HD 94012 which have nearly identical $[\text{Fe}/\text{H}]$ and the same $A(\text{Be})$ and vary only slightly in age (10 Gyr vs. 8 Gyr) even though they differ in T_{eff} by 250 K. In Figure 4 are HD 199960 and HD 15335. They have the same age (6.5 Gyr), and T_{eff} ; however, they differ in both $[\text{Fe}/\text{H}]$ and $A(\text{Be})$ by a factor of two. This supports the trend of an increasing Be abundance with increasing $[\text{Fe}/\text{H}]$ for halo and disk stars (e.g. see Boesgaard & Novicki 2006 Figure 7). Finally, in Figure 5 are HD 209320 and HD 30743. These stars have the same age but differ in $[\text{Fe}/\text{H}]$ by 0.4 dex, T_{eff} by 225 K, and in $A(\text{Be})$ by 0.2 dex.

Table 4 includes the parameters such as mass, age and absolute visual magnitude as determined by LR04, including their value for $A(\text{Li})$. The final column has the Be abundance

²<http://verdi.as.utexas.edu/moog.html>

determined in this work.

In the temperature regime of our stars, an error of 100 K results in a negligible error in $A(\text{Be})$, ≤ 0.01 dex. However, an uncertainty in $\log g$ of ± 0.5 produces an error between 0.044 to 0.052 dex depending upon T_{eff} . A combination of errors due to uncertainties in T_{eff} , $\log g$, $[\text{Fe}/\text{H}]$, ξ , S/N of the observed spectrum, and the goodness-of-fit of the synthetic spectrum combine to give errors in $A(\text{Be})$ of 0.1 to 0.2 dex. There are nine stars analyzed here with Be detections that can be compared with the results in B01, B04a, and B04b. The average differences in the parameters used are $\Delta T = 5$ K, $\Delta \log g = -0.05$, $\Delta[\text{Fe}/\text{H}] = -0.03$ (in the sense of LR04 minus previous publications); these are insignificant differences. The differences in the values of $A(\text{Be})$ for the nine stars are -0.12 ± 0.12 .

4. ANALYSIS AND RESULTS

4.1. General Results

We have found Be abundances in 46 of our 50 stars ranging from $A(\text{Be}) = 0.57$ up to the meteoritic abundance of 1.42. This represents a spread in $A(\text{Be})$ of almost an order of magnitude in one solar-mass stars. The four upper limits to $A(\text{Be})$ extend this range down to < -0.2 or a factor of more than 40. In our sample there are six stars with only upper limits on the Li abundance and four of them also have only upper limits on Be, while the two others have measured Be. Two of the Li- and Be-deficient stars, HD 182101 and HD 218470, are in the Li-Be dip region of T_{eff} .

Histograms of the Li and Be abundance distributions are shown in Figure 6. For this sample of 44 Li detections of one solar-mass stars the median value of $A(\text{Li}) = 2.39$ and for the 46 Be detections the median $A(\text{Be})$ is 0.92. Both of these values are lower than their meteoritic counterparts of 3.31 and 1.42 respectively; this indicates considerable stellar depletion relative to the meteoritic values. All the stars are Li depleted and all but one are Be depleted.

When we narrow the mass range to those stars that are within ± 0.03 solar masses ($0.97 - 1.03 M_{\odot}$) and select those within ± 100 K of the Sun, there are six in our sample. For these six the mean $A(\text{Li}) = 2.24 \pm 0.23$ and the mean $A(\text{Be}) = 1.03 \pm 0.14$. These values compare well, within the errors, with the medians from the whole sample. The six stars (HD 22521, 26421, 94835, 100180, 186379, and 217877) are all older than the sun by 3-4 Gyr (except HD 94835 which is only 2.3 Gyr older) according to the G00 tracks and isochrones. Their old age and relatively high mean Li abundance, $A(\text{Li}) = 2.24$, only deepens the mystery of the large solar Li depletion, $A(\text{Li})_{\odot} \sim 1.0$.

4.2. HR Diagram

In the LR04 study, masses and ages were determined via the G00 isochrones and evolutionary tracks. We have put our Be results in the familiar context of the HR diagram by showing the relative Be abundances along with the G00 evolutionary tracks and isochrones in Figures 7 and 8. We have used tracks for $[\text{Fe}/\text{H}]$ of 0.0 and -0.4 and include stars with $[\text{Fe}/\text{H}] > -0.2$ in Figure 7 and < -0.2 in Figure 8. The evolutionary tracks that cover our range of mass of $0.9 - 1.1 M_{\odot}$ are shown for the respective values of $[\text{Fe}/\text{H}]$. Isochrones for 100, 700, 2500 and 4500 myr are also shown in each figure. The four sizes of symbols indicates the size of $A(\text{Be})$.

In Figure 8, two stars appear to be $>1.1 M_{\odot}$ for this survey, but this is due to the metallicity dependence of the evolutionary tracks; in LR04 smaller intervals were chosen for the tracks and therefore better constraints on the mass in LR04 were made. Although stars which fall near the cutoff between the two tracks in this study do not appear to be in the right mass range, the masses for these stars are indeed in the correct range and have been adopted from the LR04 paper.

As can be seen in Figure 1, many of the stars in our sample have evolved away from the zero age main sequence (which is the reason why evolutionary ages can be assigned). In S04 the cut-off between dwarfs and subgiants is given as $\log g = 4.1$. There are 17 stars in this sample that accordingly would be classified as subgiants. These stars generally have lower Be abundances with a mean $A(\text{Be})$ of 0.82 (excluding the two with upper limits). The stars with $\log g \leq 4.1$ separate out in the distribution shown in the Be histogram in the lower portion of Figure 6; the lower three bins have 3, 8, and 4 stars that are subgiants.

The evolutionarily older subgiants show typically lower Be abundances at a given T_{eff} than the dwarf stars. The older age of the subgiants allow them to have had more time for slow mixing of the light elements, leading to depletion on the main sequence while the more advanced evolutionary stage allows them to have enlarged the surface convection zones leading to light element dilution.

It may also just be a reflection of small number statistics; S04 do not see a similar depletion in their subgiants as seen in their Figure 4. Indeed there would not be as much Be dilution in evolved stars compared to Li dilution. Figures 7 and 8 show little sign of a correlation between Be abundance and evolutionary age along the mass tracks.

4.3. Trends with Temperature

This solar-mass sample was selected from a survey of F and G stars in the local thin disk. This resulted in a temperature range for our stars from 5600 to 6400 K. When plotted against temperature, an upper envelope for the Be abundance becomes apparent as seen in Figure 9. The highest Be abundances are present near 5800-600 K, with reduced amounts of Be in the hotter stars of our sample, 6300-6500 K, in the Li-Be dip region. For the Hyades this dip region is about $T_{\text{eff}} \sim 6300 - 6800$ K (e.g. Boesgaard & Tripicco 1986) but for older stars the dip region may enlarge toward cooler temperatures (e.e. Michaud 1986) and show a larger spread in $A(\text{Li})$ (e.g. Jones et al. 1999).

The lowest Be *detections* for this sample are $A(\text{Be}) \sim 0.5$ dex and the Be abundances range up to 1.42. This order of magnitude spread can be seen particularly in the cooler stars (i.e. $T_{\text{eff}} \leq 5900$ K). The stars in the S04a paper have T_{eff} in the range of 4800 to 6300 K. They find a abundance peak in $A(\text{Be})$ near 6100 K, with a gentle decline toward lower temperatures approaching 5000 K. Their sample includes planet-host stars, many of which are metal-rich, whereas our sample has only two stars with $[\text{Fe}/\text{H}] > 0.00$. Those metal-rich stars show enhanced Be. Although our sample shows no such Be abundance peak and decline we note that our sample covers a specific mass range and thus a smaller range in temperature than that of S04a; we would not expect to see the decline in Be with decreasing temperature that they found.

Both slow mixing and convection zone depth vary with the stellar metallicity at a given mass or T_{eff} . There is evidence of a correlation between $[\text{Fe}/\text{H}]$ and $A(\text{Be})$ (e.g. Boesgaard et al. 2008, Boesgaard & Novicki 2006, and §4.4 below). That correlation needs to be considered when evaluating the temperature relation. The range for metallicity for our stars is $-0.65 \leq [\text{Fe}/\text{H}] \leq +0.11$. In Figure 10 we show the Be abundances normalized to Fe as $[\text{Be}/\text{Fe}]$ versus T_{eff} . (We used the meteoritic $A(\text{Be})$ for the solar system normalization.) The normalized ratio, $[\text{Be}/\text{Fe}]$, shows some spread at a given temperature, but no dramatic trend with temperature. And unlike Figure 9, the dwarfs and subgiants show similar relations with temperature. This plot of $[\text{Be}/\text{Fe}]$ against T_{eff} does not yield the same trend as seen in S04a.

4.4. Trends with $[\text{Fe}/\text{H}]$

The stars of this sample are members of the thin disk and generally have considerably higher metallicities than those of the thick disk and halo populations. These stars are of metallicity $[\text{Fe}/\text{H}] > -0.65$, with two positive metallicity stars. However, when the Be

abundance is plotted against $[\text{Fe}/\text{H}]$ in Figure 11, the metal-rich stars of this survey match the trend with the halo stars sampled in Boesgaard et al. (2008) remarkably well. The slope of the relation between $A(\text{Be})$ and $[\text{Fe}/\text{H}]$ is 0.86 ± 0.02 . The most metal-rich star (at $[\text{Fe}/\text{H}] = 0.11$) in our sample is HD 199960 whose Be abundance is equivalent to that of the meteoritic value of 1.42 dex (Grevesse & Sauval 1998). This value is also the highest Be abundance in this sample, supporting the idea that $A(\text{Be})$ increases with $[\text{Fe}/\text{H}]$.

This is a remarkable trend, extending over nearly four orders of magnitude in $[\text{Fe}/\text{H}]$ and over three orders of magnitude in $A(\text{Be})$.

Another illustration of this relation is to sort the sample into metallicity bins. We created four metallicity bins and took the mean $A(\text{Be})$ from the three most Be-rich stars per bin. Table 5 shows again that $A(\text{Be})$ increases as $[\text{Fe}/\text{H}]$ increases. LR04 created similar $[\text{Fe}/\text{H}]$ bins for their data with the Li abundance and found that as the $[\text{Fe}/\text{H}]$ increased the Li abundance increased (which was expected), and so did the mass. Given that our data were selected based on mass, it was not possible to see the mass trend; however, we did apply the same $[\text{Fe}/\text{H}]$ bins to the 157 LR04 solar mass stars that had Li abundances. $A(\text{Li})$ is shown to increase with increasing $[\text{Fe}/\text{H}]$ as well, but it is less obvious in our smaller data set.

4.5. Trends with Age

One of the aims of this study was to understand the relationship between $A(\text{Be})$ and age. The mass constraint was placed at $1 \pm 0.1 M_{\odot}$ in order to parameterize the $A(\text{Be})$ -age relation. Of our stars, all but one are older than the 4.5 Gyr Sun, eight (or 15%) have ages < 6 Gyr and two (4%) have ages < 5 Gyr. This fits well with the larger sample of LR04 stars with masses between 0.9 and $1.1 M_{\odot}$. The full LR04 sample includes 451 stars, with 157 (or 35% of the sample) within our mass constraints; of those 157 stars, only 34 (22%) have ages < 6 Gyr and only 6 (4%) have ages < 5 Gyr.

Figure 12 plots $A(\text{Be})$ against age and $[\text{Be}/\text{Fe}]$ against age. The spread in $A(\text{Be})$ (including upper limits) is nearly 1.5 dex for the entire range of ages; including only the Be detections, the spread is still 0.9 dex. It should be noted that only one star (HD 199960) has larger $A(\text{Be})$ than the Sun with the rest being below the solar $A(\text{Be})$ value of ~ 1.3 dex (e.g. Boesgaard et al. 2003). These stars, which have evolved away from the zero age main sequence, have continued to lose Be. In the lower panel one can see that the scatter is reduced by using $[\text{Be}/\text{Fe}]$, correcting for each star’s metallicity. A small trend is found such that the older stars have more Be relative to Fe in our one-solar mass sample. The ratio of

Be/Fe is two times larger in the stars of 10 Gyr compared to those of 5 Gyr.

4.6. Trends with Lithium Abundance

Understanding the correlation between Be and Li is key to understanding the nature of light element depletion and slow mixing in these stars. Figure 13 shows the plot of $A(\text{Be})$ versus $A(\text{Li})$.

B05 found a linear relationship between $A(\text{Li})$ and $A(\text{Be})$ for field and cluster stars in the T_{eff} ranges of 5900-6300 K (the Li “plateau”) and 6300-6650 K (the cool side of the Li-dip) with slopes of 0.365 ± 0.036 and 0.404 ± 0.034 respectively. We can combine our data with the field stars of B04 in the temperature range of $5900 < T_{\text{eff}} < 6300$ K. Figure 13 shows those results for the total of 60 stars. The triangles are stars from this study. For the combined data we find a slope of 0.34 ± 0.05 which compares well with the slope for 31 field stars in this same temperature range in B04: 0.36 ± 0.05 . Note that the three most Li- and Be-depleted stars in Figure 13 all have solar metallicity: $[\text{Fe}/\text{H}] = -0.03, +0.09, +0.12$. It appears that metallicity is not an important factor in the Li-Be correlation.

4.7. The Spread in Be Abundance

There is clear evidence that astration of Be is taking place in these one-solar-mass stars. The spread in $A(\text{Be})$ and $[\text{Be}/\text{Fe}]$ at a given temperature shows that. The spread in $A(\text{Be})$ covers more than 1.5 dex, while the typical errors are ± 0.15 . There are two stars in our sample that have nearly identical stellar parameters, yet they differ in both $A(\text{Be})$ and $A(\text{Li})$ by a factor of two. The Be region of the spectra of these two stars, HD 200580 and HD 204712, are shown in Figure 14. Only the two Be II lines show meaningful differences between these two spectra. Their full set of stellar parameters are given in Table 4. They differ in T_{eff} by only 35 K, in $\log g$ by 0.07, and in $[\text{Fe}/\text{H}]$ by only 0.06, all within the precision of their determinations. Their respective masses are 0.95 and 0.96 M_{\odot} and their ages are 9.17 and 9.35 Gyr, with the slightly older one having more Be.

This pair may indicate that another parameter plays a role in Be astration; it has been suggested by B04a that rotational velocity is that parameter. Stars are formed with differing initial velocities and spin down to their present-day values. During the spin-down, extra mixing occurs which increases the amount of Be (and Li) that can reach the critical temperature for destruction. As found by B04a the depletion of Li and Be observed in cluster and field stars is well-matched by the rotation-model predictions of Deliyannis &

Pinsonneault (1997). See Figure 12 of B04a.

5. SUMMARY AND CONCLUSIONS

We have determined Be abundances for 50 solar-mass stars using spectra taken at the Keck I telescope and the CFH Telescope. The stars were selected from LR04 to be within $0.1 M_{\odot}$ of the sun. Most of our sample of one-solar-mass stars were taken using the new Keck I HIRES mosaic CCD, the resolution was $\sim 78,000$ with a median S/N ratio of 146. The data were reduced using the IDL HIRES Redux pipeline and IRAF. We adopted the stellar parameters as determined by LR04 and used them to create model atmospheres for spectral synthesis in MOOG using the Kurucz grid point models. Be abundances were determined by fitting the 4 \AA region around the Be II resonance lines located at 3130.421 and 3131.065 \AA . We plotted HR diagrams using the G00 isochrones and evolutionary tracks in combination with the LR04 stellar parameters. The majority of our stars are evolved away from the zero age main sequence and all but one are older than the Sun.

The main results from our analysis are as follows:

In spite of the similarity in mass of our stars, there is a wide range in Be abundances from $A(\text{Be}) < -0.2$ to $+1.42$, or more than a factor of 40. The median Be abundance is 0.92 – for the 46 stars with Be detections – which represents a deficiency relative to the meteoritic abundance of $A(\text{Be}) = 1.42$. The median Li abundance for the 44 stars with Li detections is $A(\text{Li}) = 2.39$, also deficient compared to the meteoritic value of 3.31. See Figure 6 for the distribution of light elements in our stars. Of our four stars with upper limits on the Be abundances, all have upper limits on Li also. This is expected since Li is destroyed in stellar interiors at lower temperatures than Be by (p,α) , making Li more susceptible to destruction.

We have compared the positions of our stars on the HR diagram with the isochrones and evolutionary tracks of G00 (see Figures 7 and 8). In our sample of 50 stars the subgiants, as defined by $\log g < 4.1$, make up one-third of the stars. At a given T_{eff} these more-evolved stars generally have lower Be abundances than the main-sequence stars. The reduced amount of Be could result both from more depletion on the main sequence and possibly from more dilution due to the expansion of the surface convection zone in the evolutionarily more advanced subgiants.

This one-solar-mass sample of thin disk stars matches the remarkable relationship between $A(\text{Be})$ and $[\text{Fe}/\text{H}]$ found earlier (e.g. Boesgaard et al. 1999, Boesgaard & Novicki 2006, Boesgaard et al. 2008). As can be seen in Figure 11, this relationship extends over 4 orders of magnitude in $[\text{Fe}/\text{H}]$ and more than 3 orders of magnitude in $A(\text{Be})$. The linear

relation between these two logarithmic quantities has a slope of 0.86 ± 0.02 . This indicates an increase in the abundance of both elements over the age of the Galaxy even though Fe is made by nuclear processing in stars and Be is made through spallation reactions outside of stars.

In the relation between $A(\text{Be})$ and T_{eff} there are lower Be abundances near the F star Li-Be dip, while the higher Be abundances appear in the cooler stars, as can be seen in Figure 9. In fact, there is a large spread in $A(\text{Be})$ in the cooler stars. Due to the relationship between $A(\text{Be})$ and $[\text{Fe}/\text{H}]$, we have normalized the Be abundances to the Fe abundances and form $[\text{Be}/\text{Fe}]$. When this parameter is plotted against T_{eff} (see Figure 10), there is no temperature dependence. The main sequence stars and the subgiants have similar distributions of $[\text{Be}/\text{Fe}]$ with T_{eff} . Even with this normalization, however, there is a large spread in $[\text{Be}/\text{Fe}]$ of a factor of 6 (not including the upper limits on Be).

The spread that we find is larger than the typical error of ~ 0.12 dex in the Be abundances. We can see this in the pair of nearly identical stars, HD 200580 and HD 204712, which differ in Be abundance by a factor of 2 although they have the same $[\text{Fe}/\text{H}]$, T_{eff} , $\log g$, age and mass. See Figure 14.

The range in age of our stars in the one-solar-mass sample covers 3.8 to 9.9 Gyr. In this age range there is a spread of 1.5 dex in $A(\text{Be})$. However, as can be seen in Figure 12, there is no noticeable trend of Be abundance with age. All except one of our stars are older than the sun and all, except one, have lower Be abundances than that found in meteorites (and in the Sun). The stellar deficiencies in Be are probably indicative of the longer time over which slow mixing and depletion of Be has taken place. For the stars that have evolved toward the base of the red giant branch, the deepening of the surface convection zone could have produced additional dilution of the surface Be content.

Of our 50 stars, 30 are in the temperature regime of $T_{\text{eff}} = 5900 - 6300$ K. This range corresponds to the “Li plateau” region in the Hyades cluster (see B04a). This doubles the number of field stars with detectable Li and Be and confirms the linear correlation of $A(\text{Li})$ and $A(\text{Be})$. The slope is $+0.34 \pm 0.05$ for the 60 stars in this temperature region for main-sequence and subgiant stars. The Li depletion is more severe than the Be depletion, as expected. The observed characteristics are in excellent agreement with the predictions of rotational mixing by Deliyannis & Pinsonneault (1997).

We are grateful to the Keck Observatory support astronomers, Grant Hill, Jeffrey Mader, Hien Tran, and Greg Wirth for their assistance with HIRES and to Megan Novicki and Jeffrey Rich for help in the data reduction. JAK was supported through NSF-Research Experiences for Undergraduates program to the University of Hawaii grant AST 04-53395. This work

was supported by NSF AST 05-05899 to AMB.

REFERENCES

- Balachandran, S. 1990, ApJ, 354, 310
- Boesgaard, A. M., Armengaud, E. & King, J. R. 2003, ApJ, 582, 410
- Boesgaard, A. M., Armengaud, E., King, J. R., Deliyannis, C. P., & Stephens, A. 2004a, ApJ, 613, 1202 (B04a)
- Boesgaard, A.M., Deliyannis, C.P. & Steinhauer, A. 2005, ApJ, 621, 991
- Boesgaard, A.M., Deliyannis, C.P., King, J.R., Ryan, S.G., Vogt, S.S. & Beers, T.C. 1999, AJ, 117, 1549
- Boesgaard, A. M., Deliyannis, C. P., King, J. R., & Stephens, A. 2001, ApJ, 553, 754
- Boesgaard, A. M. & King, J. R. 2002, ApJ, 565, 587
- Boesgaard, A. M., McGrath, E. J., Lambert, D. L., & Cunha, K. 2004b, ApJ, 606, 306 (B04b)
- Boesgaard, A. M., & Novicki, M. C. 2006, ApJ, 641, 1122
- Boesgaard, A. M., Rich, J., & Levesque, E. 2008, in *The First Stars, III*, eds. B.W. O’Shea, A. Heger, & T. Abel, (AIP), p. 164
- Boesgaard, A. M., & Tripicco, M. J. 1986, ApJ, 303, 724
- Chen, Y. Q., Nissen, P. E., Benoni, T., & Zhao, G. 2001, A&A, 371, 943
- Deliyannis, C.P. & Pinsonneault, M.H. 1997, ApJ, 488, 836
- Edvardsson, B., Andersen, J., Gustafsson, B., Lambert, D. L., Nissen, P. E., & Tomkin, J. 1993, A&A, 275, 101
- Girardi, L., Bressan, A., Bertelli, G., & Chiosi, C. 2000, A&AS, 141, 371
- Grevesse, N., & Sauval, A. J. 1998, Space Science Reviews, 85, 161
- Jones, B.F., Fischer, D & Soderblom, D.R. 1999, AJ, 117, 330
- Kurucz, R. L. 1993, VizieR Online Data Catalog, 6039, 0
- Lambert, D. L., & Reddy, B. E. 2004, MNRAS, 349, 757 (LR04)
- Michaud, M. 1986, ApJ, 302, 650
- Montalbán, J., & Schatzman, E. 2000, A&A, 354, 943
- Pinsonneault, M. H., Kawaler, S.D. & Demarque, P. 1990, ApJS, 74, 501

- Pinsonneault, M. H., Deliyannis, C. P., & Demarque, P. 1992, *ApJS*, 78, 179
- Reddy, B. E., Tomkin, J., Lambert, D. L., & Allende Prieto, C. 2003, *MNRAS*, 340, 304
- Santos, N. C., Israelian, G., Randich, S., García López, R. J., & Rebolo, R. 2004a, *A&A*, 425, 1013 (S04a)
- Santos, N. C., Israelian, G., García López, R. J., Mayor, M., Rebolo, R. Randich, S., Ecuillon, A. & Domnguez Cerdea, C. 2004b, *A&A*, 427, 1085
- Snedden, C. 1973, *ApJ*, 184, 839
- van Dokkum, P. G. 2001, *PASP*, 113, 1420
- Vogt, S. S. et al. 1994, *Proc. SPIE*, 2198, 362

Table 1. Keck HIRES Observations

Star HD	Star HR	V	Night	Exp. Time (min)	Total S/N
HD 5494	...	7.95	02 Jan 2006	7	267
HD 14877	...	8.46	31 Jan 2005	8	107
HD 22521	...	6.95	31 Jan 2005	4	146
HD 24421	...	6.83	31 Jan 2005	4	148
HD 25173	...	7.16	31 Jan 2005	8	53
HD 26421	...	8.19	31 Jan 2005	10	127
HD 28620	...	6.81	31 Jan 2005	8	226
HD 30743	HR 1545	6.26	27 Sep 2005	3	208
HD 33632	...	6.46	31 Jan 2005	6	226
HD 35296	HR 1780	5.00	11 Jan 2007	20	40
HD 54717	...	7.20	01 Apr 2005	25	71
HD 63333	...	7.11	01 Apr 2005	20	47
HD 68284	...	7.78	01 Apr 2005	60	76
HD 78418	HR 3626	5.98	11 Jan 2007	5	115
HD 80218	...	6.63	01 Apr 2005	15	78
HD 87838	...	7.73	11 Jan 2007	30	59
HD 88446	...	7.85	11 Jan 2007	30	33
HD 89125	HR 4039	5.80	01 Apr 2005	15	204
HD 91638	...	6.68	01 Apr 2005	25	133
HD 91889	HR 4158	5.70	02 Jan 2006	4	350
HD 94012	...	7.85	11 Jan 2007	30	113
HD 94835	...	7.96	01 Apr 2005	30	252
HD 100180	HR 4437	6.20	01 Apr 2005	20	330
HD 101676	...	7.09	11 Jan 2007	25	197
HD 108510	...	6.69	11 Jan 2007	25	260
HD 108845	HR 4761	6.21	09 Jun 2007	3	273
HD 109303	...	8.15	09 Jun 2007	15	289
HD 112756	...	8.15	11 Jan 2007	20	126
HD 118244	...	6.99	02 Jan 2006	5	235
HD 121560	HR 5243	6.10	11 Jan 2007	7	146

Table 1—Continued

Star HD	Star HR	V	Night	Exp. Time (min)	Total S/N
HD 169359	...	7.81	06 Jul 2005	7	110
HD 186379	...	6.76	27 Sep 2005	5	257
HD 200580	...	7.33	09 Jun 2007	6	277
HD 202884	...	7.27	18 Nov 2004	4	122
HD 204712	...	7.65	09 Jun 2007	6	252
HD 209320	...	8.32	02 Jan 2006	5	150
HD 209858	...	7.79	18 Nov 2004	10	148
HD 215442	...	7.53	18 Nov 2004	7	124
HD 217877	HR 8772	6.68	05 Jul 2005	5	173
HD 221356	HR 8931	6.49	05 Jul 2005	5	188

Table 2. Observations

Star HD	HR	V	Night	Exp. Time (min)	Total S/N	Telescope	Ref. ¹
HD 693	HR 33	4.89	05 Jan 2002	5	145	Keck I HIRES	B04a
HD 4813	HR 235	5.19	16 Oct 1995	15	72	CFHT Gecko	B01
HD 11592	...	6.78	16 Oct 1995	45	48	CFHT Gecko	B04b
HD 15335	HR 720	5.88	15 Nov 1999	10	108	Keck I HIRES	B04a
HD 58551	HR 2835	6.54	05 Jan 2002	12	145	Keck I HIRES	B04a
HD 58855	HR 2849	5.37	15 Oct 1995	20	88	CFHT Gecko	B01
HD 103799	HR 4572	6.62	04 Jan 2002	10	140	Keck I HIRES	B04a
HD 142860	HR 5933	3.85	16 Jul 1992	5	52	CFHT f/8 Coudé	B04b
HD 182101	HR 7354	6.35	15 Oct 1995	30	73	CFHT Gecko	B01
HD 199960	HR 8041	6.20	13 Nov 1999	12	93	Keck I HIRES	B04a
HD 218470	HR 8805	5.70	15 Oct 1995	25	79	CFHT Gecko	B01

¹B01=Boesgaard et al. 2001, B04a=Boesgaard et al. 2004a, B04b=Boesgaard et al. 2004b

Table 3. Stellar Parameters

Star	T_{eff}	$\log g$	[Fe/H]	ξ
HD 693	6132	4.12	-0.48	1.85
HD 4813	6286	4.34	-0.15	1.58
HD 5494	6082	4.00	-0.17	1.97
HD 11592	6234	4.20	-0.35	1.83
HD 14877	5970	4.03	-0.42	1.84
HD 15335	5785	3.92	-0.22	1.83
HD 22521	5783	3.96	-0.25	1.78
HD 24421	5987	4.14	-0.38	1.71
HD 25173	5867	4.07	-0.62	1.70
HD 26421	5737	3.98	-0.39	1.72
HD 28620	6101	4.08	-0.52	1.88
HD 30743	6222	4.15	-0.62	1.88
HD 33632	5962	4.30	-0.23	1.48
HD 35296	6015	4.24	-0.14	1.60
HD 54717	6350	4.26	-0.44	1.84
HD 58551	6149	4.22	-0.54	1.73
HD 58855	6286	4.31	-0.31	1.73
HD 63333	6057	4.23	-0.39	1.65
HD 68284	5832	3.91	-0.56	1.88
HD 78418	5625	3.98	-0.26	1.63
HD 80218	6092	4.16	-0.28	1.77
HD 87838	6019	4.29	-0.43	1.54
HD 88446	5875	4.08	-0.52	1.70
HD 89125	6038	4.25	-0.36	1.61
HD 91638	6159	4.29	-0.25	1.65
HD 91889	6051	4.20	-0.28	1.68
HD 94012	6064	4.41	-0.47	1.42
HD 94835	5814	4.43	+0.05	1.19
HD 100180	5866	4.12	-0.11	1.64
HD 101676	6102	4.09	-0.47	1.87
HD 103799	6169	4.02	-0.45	2.01

Table 3—Continued

Star	T_{eff}	$\log g$	[Fe/H]	ξ
HD 108510	5929	4.31	−0.06	1.44
HD 108845	6060	4.08	−0.24	1.84
HD 109303	5904	4.05	−0.52	1.76
HD 112756	5993	4.40	−0.35	1.37
HD 118244	6234	4.13	−0.55	1.92
HD 121560	6059	4.35	−0.38	1.49
HD 142860	6227	4.18	−0.22	1.85
HD 169359	5810	4.12	−0.31	1.59
HD 182101	6344	4.22	−0.29	1.89
HD 186379	5811	3.99	−0.43	1.76
HD 199960	5750	4.17	+0.11	1.48
HD 200580	5853	4.05	−0.54	1.72
HD 202884	6141	4.36	−0.24	1.55
HD 204712	5888	4.12	−0.48	1.65
HD 209320	5994	4.14	−0.18	1.71
HD 209858	5911	4.26	−0.27	1.49
HD 215442	5872	3.38	−0.22	2.60
HD 217877	5872	4.28	−0.18	1.43
HD 218470	6495	4.06	−0.13	2.22
HD 221356	6005	4.42	−0.24	1.36

Table 4. Stellar Parameters and Abundances

Star	[Fe/H]	T _{eff}	M _V	Mass	Age	A(Li)	A(Be)
HD 693	−0.48	6132	3.51	1.04	6.11	2.39	0.88
HD 4813	−0.15	6146	4.23	1.07	3.81	2.74	1.07
HD 5494	−0.17	6082	3.22	1.04	8.85	<1.04	0.57
HD 11592	−0.35	6234	3.66	1.05	5.77	2.33	0.87
HD 14877	−0.42	5970	3.67	0.98	8.34	2.39	0.77
HD 15335	−0.22	5785	3.45	1.08	6.82	2.39	1.07
HD 22521	−0.25	5783	3.60	1.03	8.10	2.53	1.00
HD 24421	−0.38	5987	3.81	0.98	8.46	2.56	1.00
HD 25173	−0.62	5867	3.52	0.96	8.63	2.49	...
HD 26421	−0.39	5737	3.68	0.98	9.02	1.91	0.87
HD 28620	−0.52	6101	3.61	0.98	7.75	2.40	0.70
HD 30743	−0.62	6222	3.53	1.00	6.54	2.35	0.81
HD 33632	−0.23	5962	4.40	0.97	7.59	2.45	0.90
HD 35296	−0.14	6015	4.15	1.02	7.12	2.87	0.97
HD 54717	−0.44	6350	3.86	1.04	5.34	2.34	0.69
HD 58551	−0.54	6149	4.09	0.92	9.14	2.49	0.81
HD 58855	−0.31	6286	3.87	1.07	5.00	2.22	0.92
HD 63333	−0.39	6057	3.92	0.97	8.52	2.38	0.85
HD 68284	−0.56	5832	3.41	1.00	7.22	2.39	0.74
HD 78418	−0.26	5625	3.48	1.07	6.73	2.03	1.00
HD 80218	−0.28	6092	3.65	1.04	6.87	<1.02	<−0.18
HD 88446	−0.52	5875	3.68	0.94	9.62	0.85	0.52
HD 87838	−0.43	6019	4.21	0.91	10.2	2.37	1.12
HD 89125	−0.36	6038	4.03	0.98	7.97	2.38	0.99
HD 91638	−0.25	6159	3.93	1.02	7.07	2.55	1.02
HD 91889	−0.28	6051	3.76	1.03	7.05	2.47	0.88
HD 94012	−0.47	6064	4.38	0.90	9.78	2.46	1.02
HD 94835	+0.05	5814	4.47	1.02	6.88	2.11	1.24
HD 100180	−0.11	5866	4.44	0.98	8.01	2.43	0.92
HD 101676	−0.47	6102	3.64	0.99	7.83	2.38	0.84
HD 103799	−0.45	6169	3.29	1.07	6.06	2.18	0.87

Table 4—Continued

Star	[Fe/H]	T_{eff}	M_V	Mass	Age	A(Li)	A(Be)
HD 108510	−0.06	5929	4.44	1.02	6.45	2.39	1.27
HD 108845	−0.24	6060	2.94	1.08	7.25	1.98	0.83
HD 109303	−0.52	5904	3.55	0.98	8.46	<1.65	0.85
HD 112756	−0.35	5993	4.52	0.92	8.99	2.46	1.10
HD 118244	−0.55	6234	3.71	0.97	7.77	2.07	0.74
HD 121560	−0.38	6059	4.24	0.95	8.70	2.43	1.01
HD 142860	−0.22	6227	3.63	1.09	5.53	2.15	0.82
HD 169359	−0.31	5810	3.91	0.96	9.71	2.33	0.87
HD 182101	−0.29	6344	3.58	1.09	5.11	<1.88	<0.65
HD 186379	−0.43	5811	3.60	0.99	8.06	2.30	1.02
HD 199960	+0.11	5750	4.10	1.08	6.48	2.37	1.42
HD 200580	−0.54	5853	3.57	0.96	9.17	2.08	0.65
HD 202884	−0.24	6141	4.15	1.03	5.57	2.63	0.92
HD 204712	−0.48	5888	3.71	0.95	9.35	2.42	0.95
HD 209320	−0.18	5994	3.78	1.05	6.87	2.45	1.02
HD 209858	−0.27	5911	4.06	0.97	8.88	2.36	0.96
HD 215442	−0.22	5872	2.96	1.00	9.86	<0.85	<0.30
HD 217877	−0.18	5872	4.24	0.97	9.24	2.16	1.14
HD 218470	−0.13	6495	3.04	1.09	7.66	<1.52	<0.1
HD 221356	−0.24	6005	4.41	0.98	6.44	2.50	1.10

Table 5. Mean Be abundances calculated from the three most Be-rich and mean Li abundances from the six most Li-rich stars in each [Fe/H] bin.

[Fe/H]	A(Be)	A(Li)
+0.2 to -0.1	1.31	2.58
-0.1 to -0.3	1.10	2.91
-0.3 to -0.5	1.08	2.63
-0.5 to -0.7	0.82	2.49

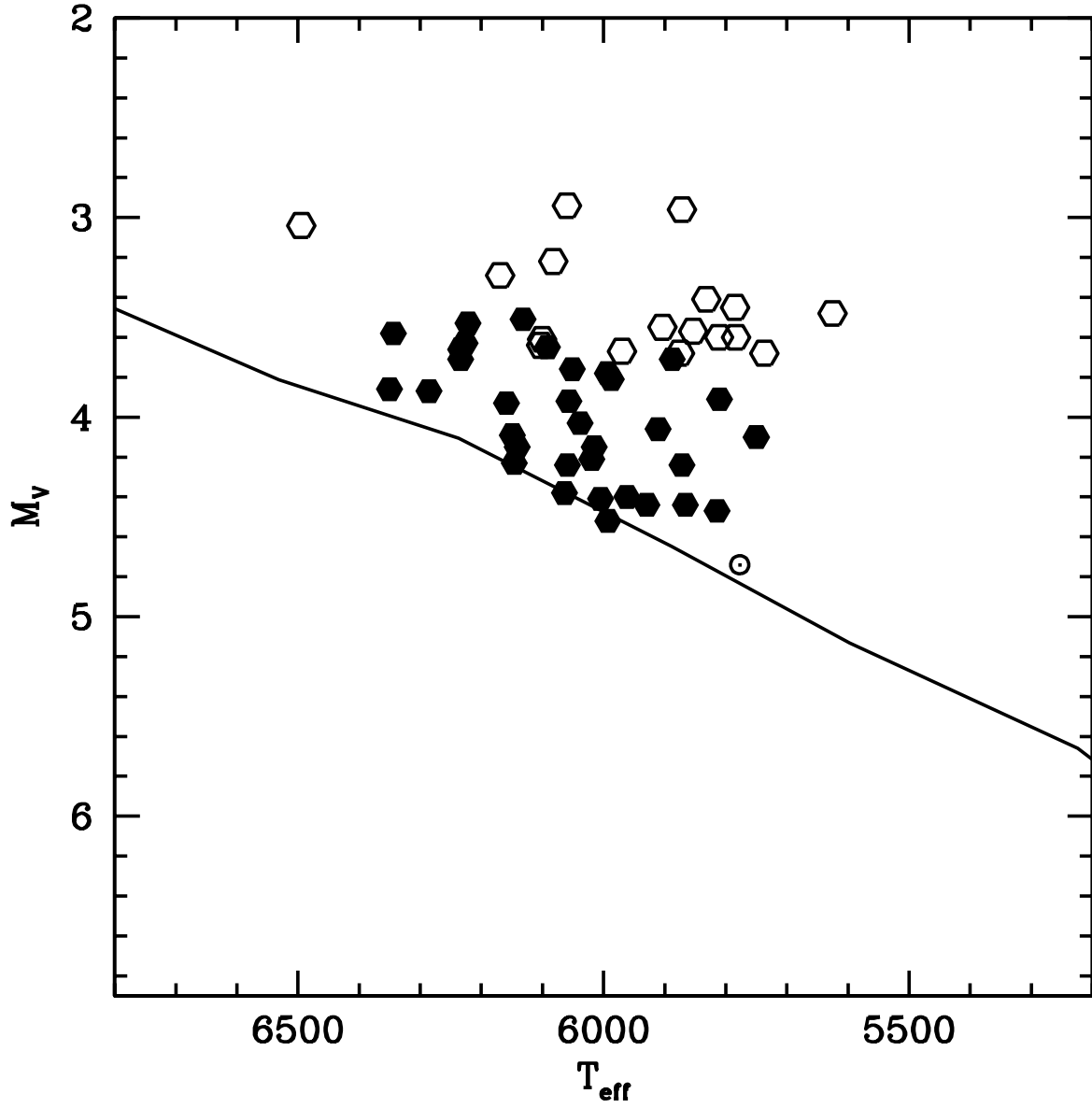


Fig. 1.— HR Diagram of the program stars plotted with the zero-age main sequence (from Girardi et al. 2000). The dwarf stars ($\log g > 4.1$) are filled hexagons and the subgiants are open hexagons. The dotted circle represents the Sun.

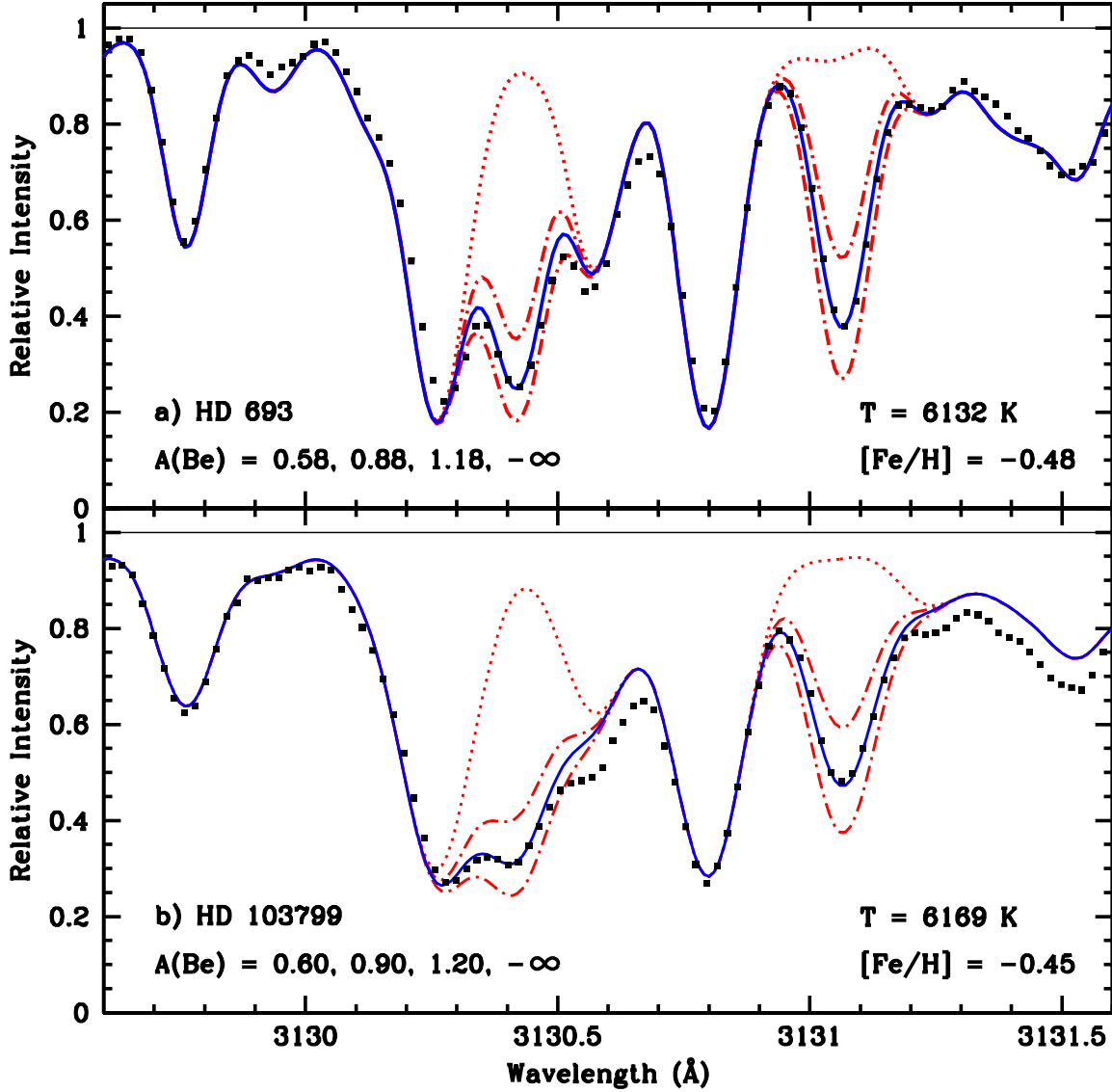


Fig. 2.— Figures 2-5 show spectral syntheses of the Be II region for selected stars of our sample. The data (points) and best fit (solid line) are shown, as well as the fits for a factor of two above and below the best fit for $A(\text{Be})$ (dashed-dotted lines) and the fit for a star with zero Be. HD 693 and HD 103799 have the same $A(\text{Be})$, T_{eff} , $[\text{Fe}/\text{H}]$, and age, but differ in rotation with HD 693 having a FWHM gaussian at 0.09 and HD 103799 at 0.13

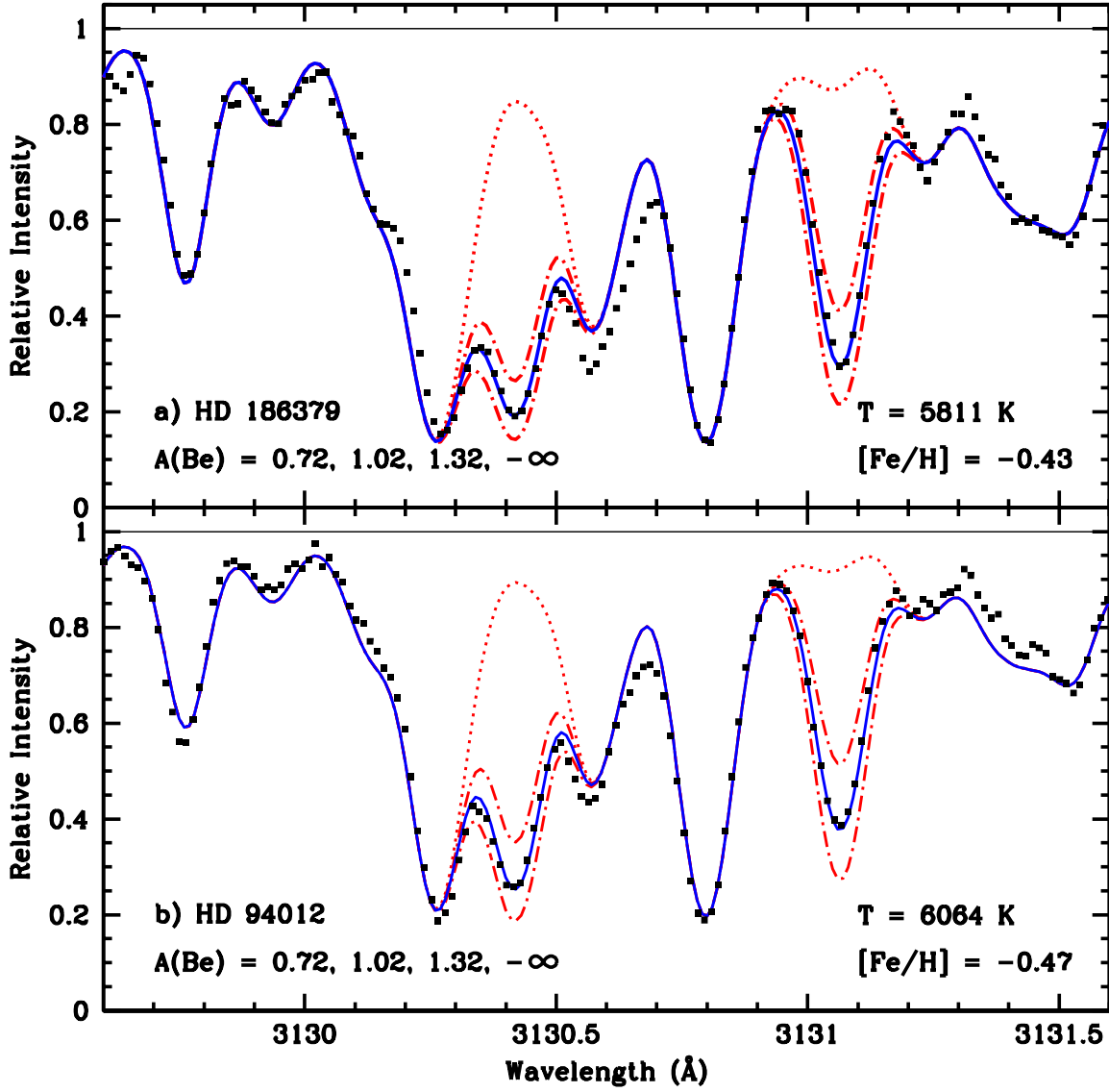


Fig. 3.— These stars are of similar $A(\text{Be})$ and $[\text{Fe}/\text{H}]$, but differ in age (10 Gyr vs 8 Gyr) and T_{eff} by 250 K. The Be abundance is the same in spite of the differences in age and T_{eff} .

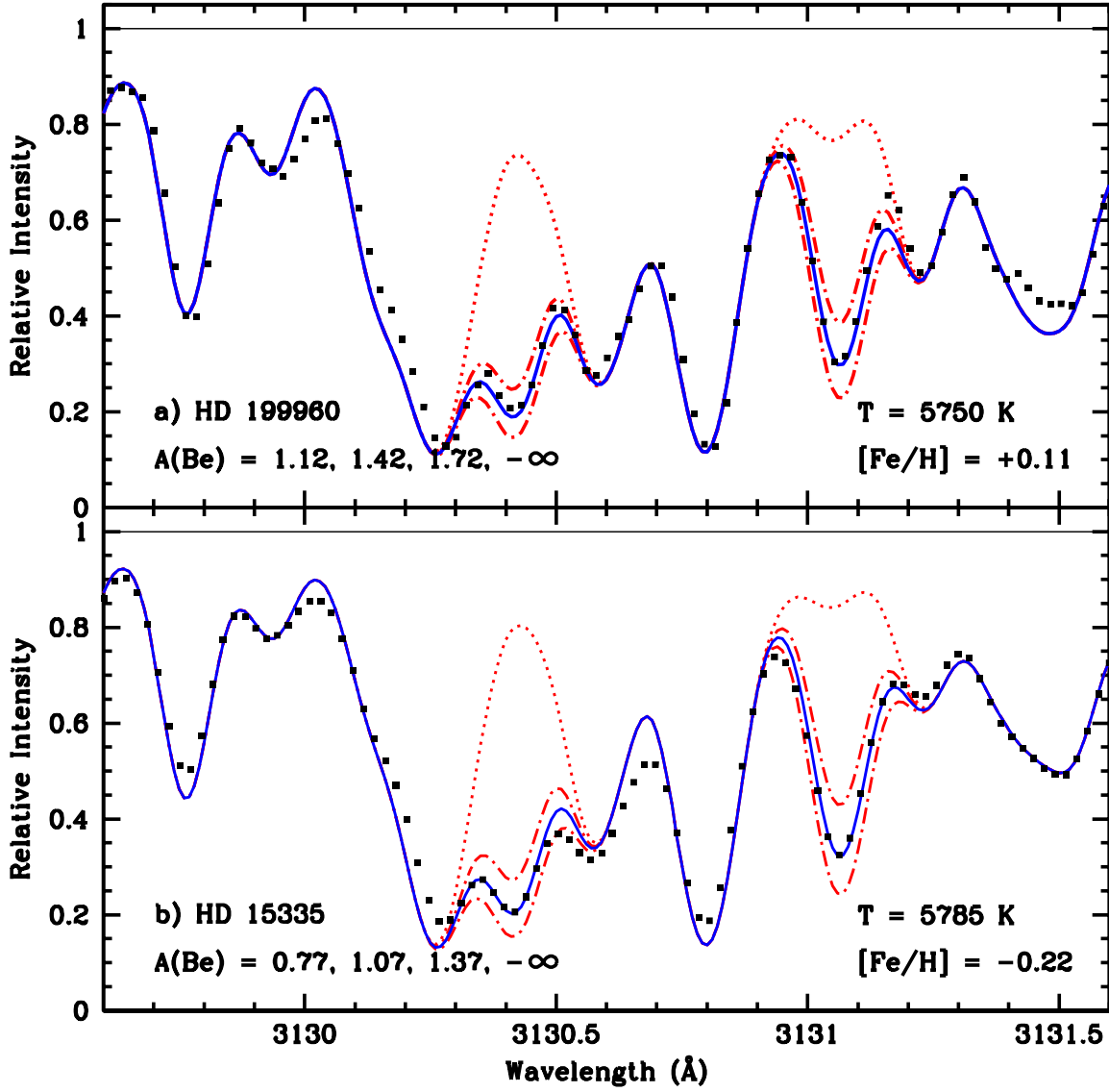


Fig. 4.— These solar temperature stars are the same age. Both $A(\text{Be})$ and $[\text{Fe}/\text{H}]$ are higher by a factor of ~ 2 in HD 199960 which is the most Be-rich star in this sample.

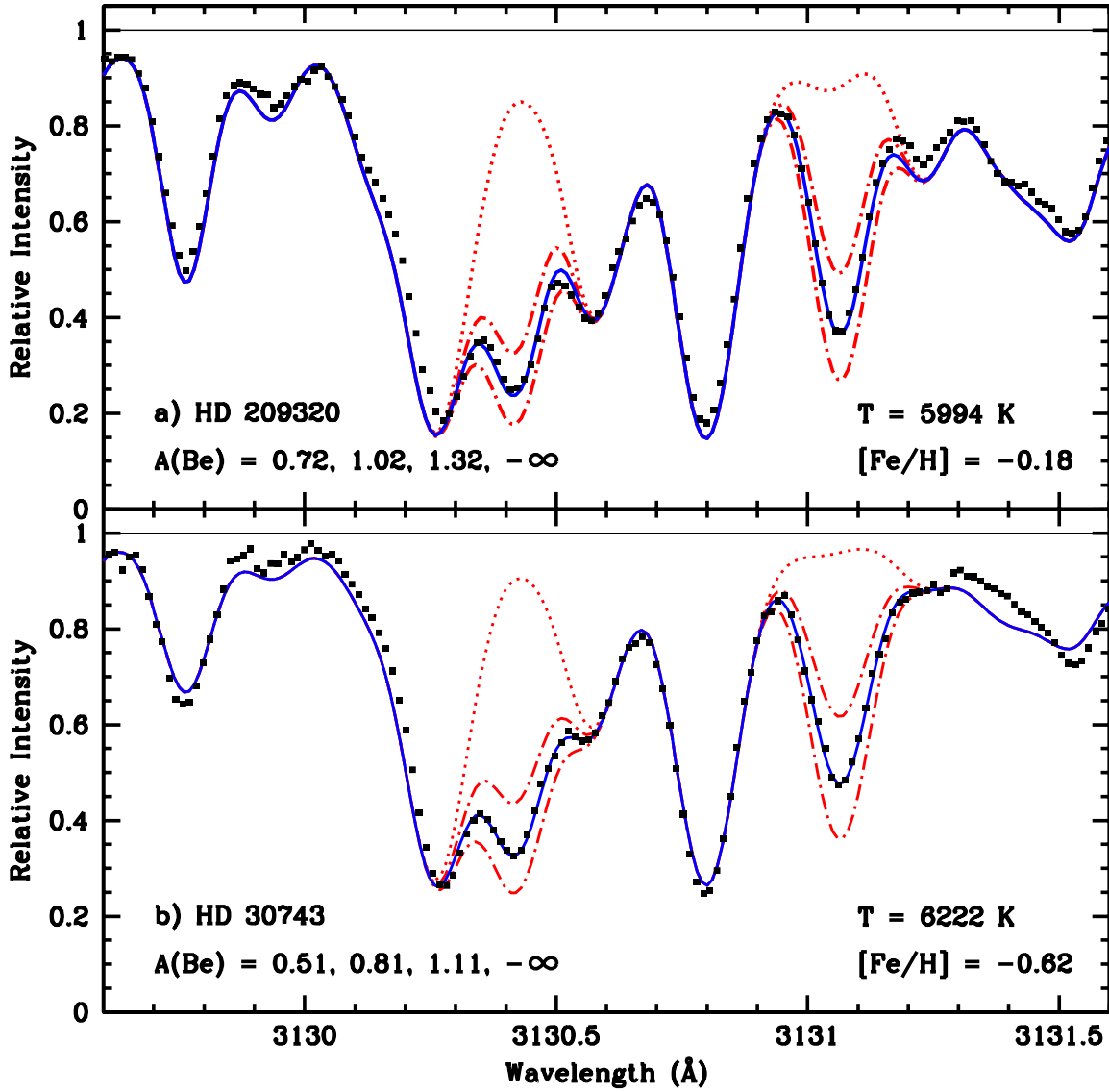


Fig. 5.— These stars have the same age at ~ 6.6 Gyr, but differ in T_{eff} , $[\text{Fe}/\text{H}]$, and $A(\text{Be})$. Iron and Be are higher by a factor of 2.7 and 1.6 respectively in HD 209320. This corresponds well to the trend shown in Figure 11.

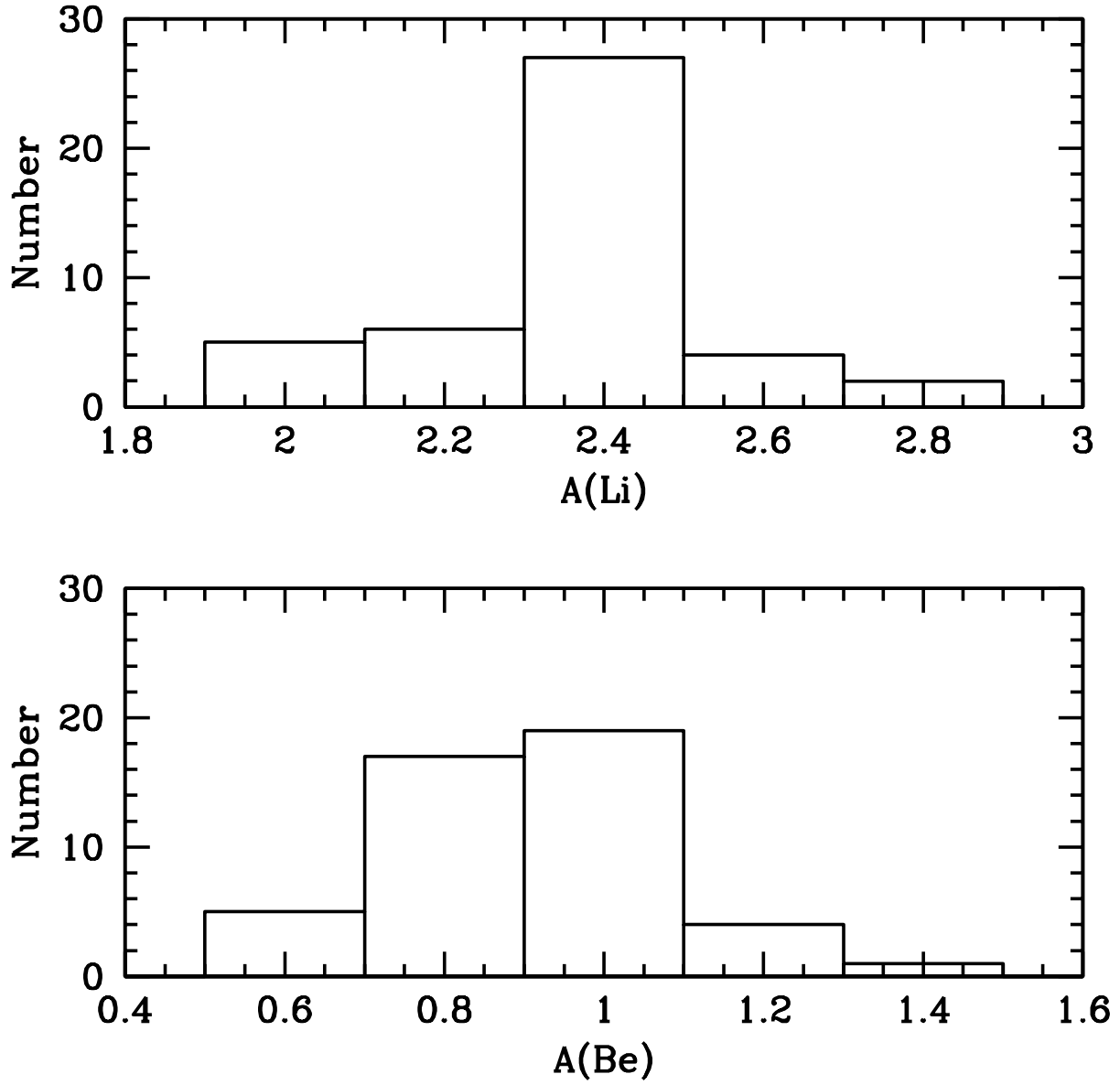


Fig. 6.— Histograms of the abundances of Li (top) and Be (bottom). For the 44 stars with Li detections the median $A(\text{Li})$ is 2.39 while for the 46 stars with Be detections the median is $A(\text{Be})$ is 0.92. The meteoritic values are 3.31 and 1.42 respectively.

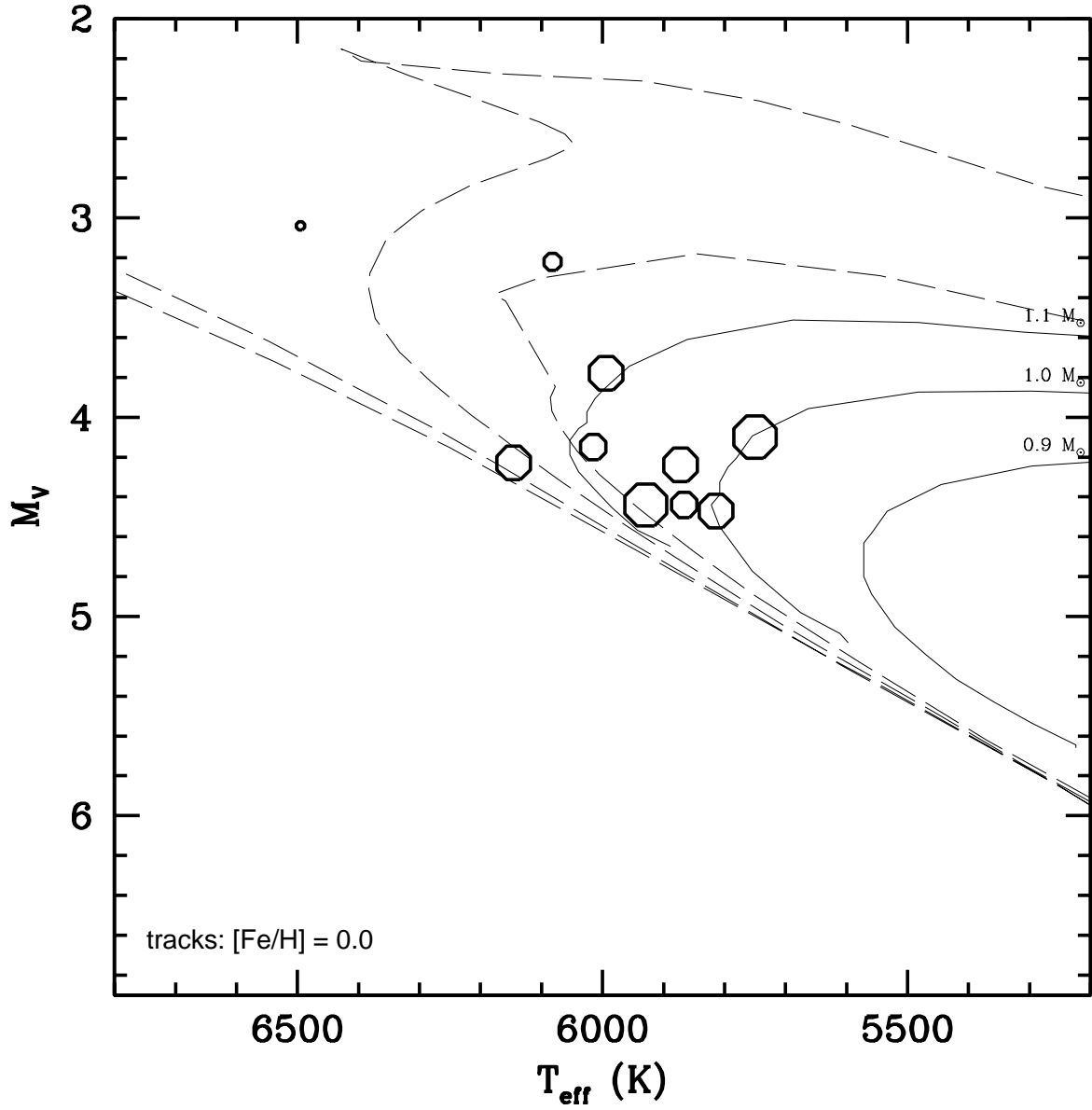


Fig. 7.— HR diagram for the 10 stars with $[\text{Fe}/\text{H}] > -0.2$. Metallicity dependent isochrones (dashed lines) for 100, 700, 2500, and 4500 Myr and evolutionary tracks (solid lines) for $[\text{Fe}/\text{H}] = 0$ from Girardi et al. (2000) are plotted. The symbol size denotes the relative amounts of Be in each star, with the largest symbols indicative of stars with $A(\text{Be}) > 1.25$ dex and subsequent smaller sizes corresponding to $A(\text{Be})$ bins of 0.25 dex.

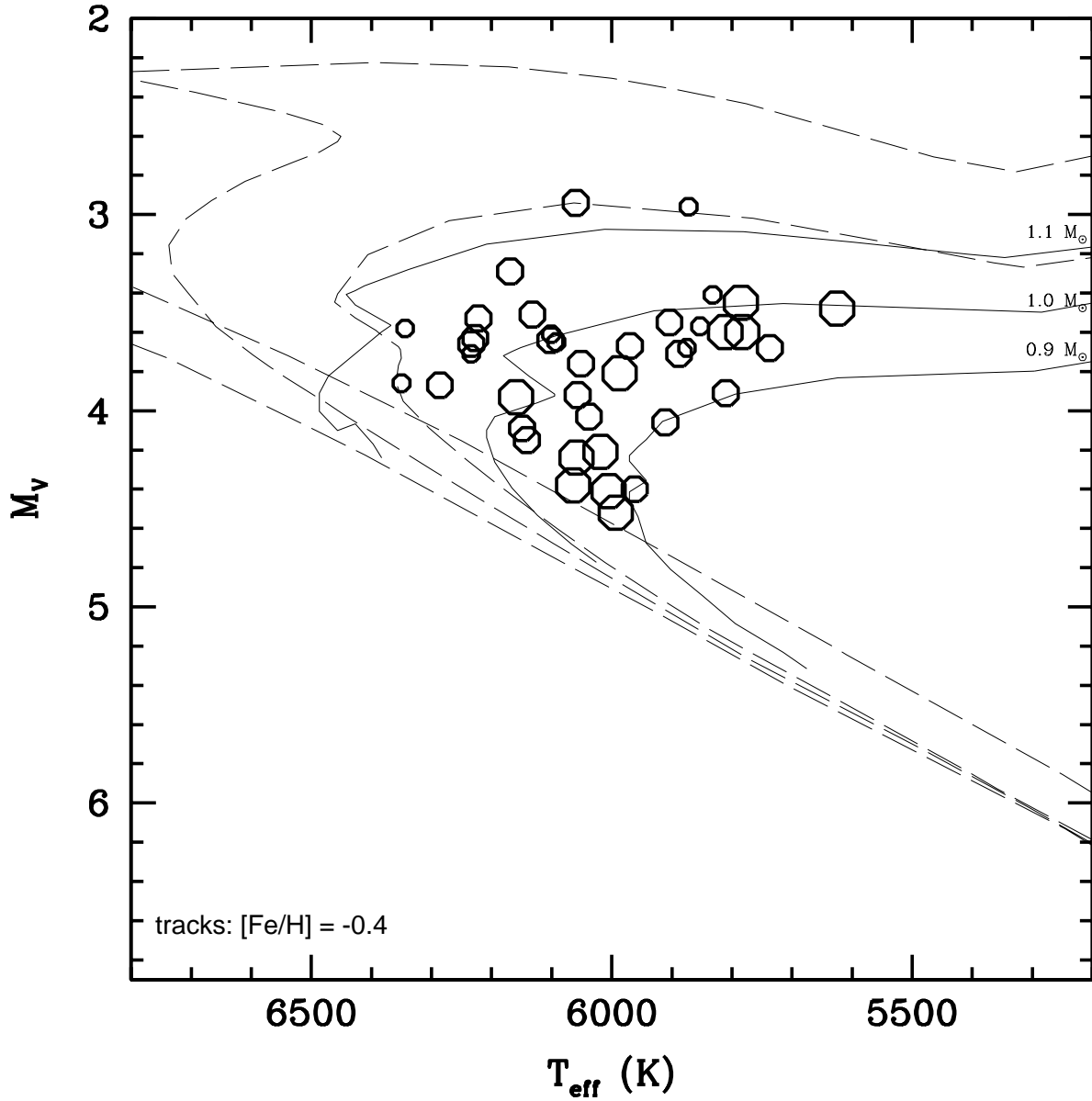


Fig. 8.— HR diagram for stars with $[\text{Fe}/\text{H}] < -0.2$. Metallicity dependent isochrones (dashed lines) for 100, 700, 2500, and 4500 Myr and evolutionary tracks (solid lines) for $[\text{Fe}/\text{H}] = -0.4$ from Girardi et al. (2000) are plotted. As in Figure 7, the symbol size indicates the relative amount of Be. In this case the largest symbol corresponds to $1.25 \leq A(\text{Be}) < 1.00$ and the smallest indicates $A(\text{Be}) < 0.75$.

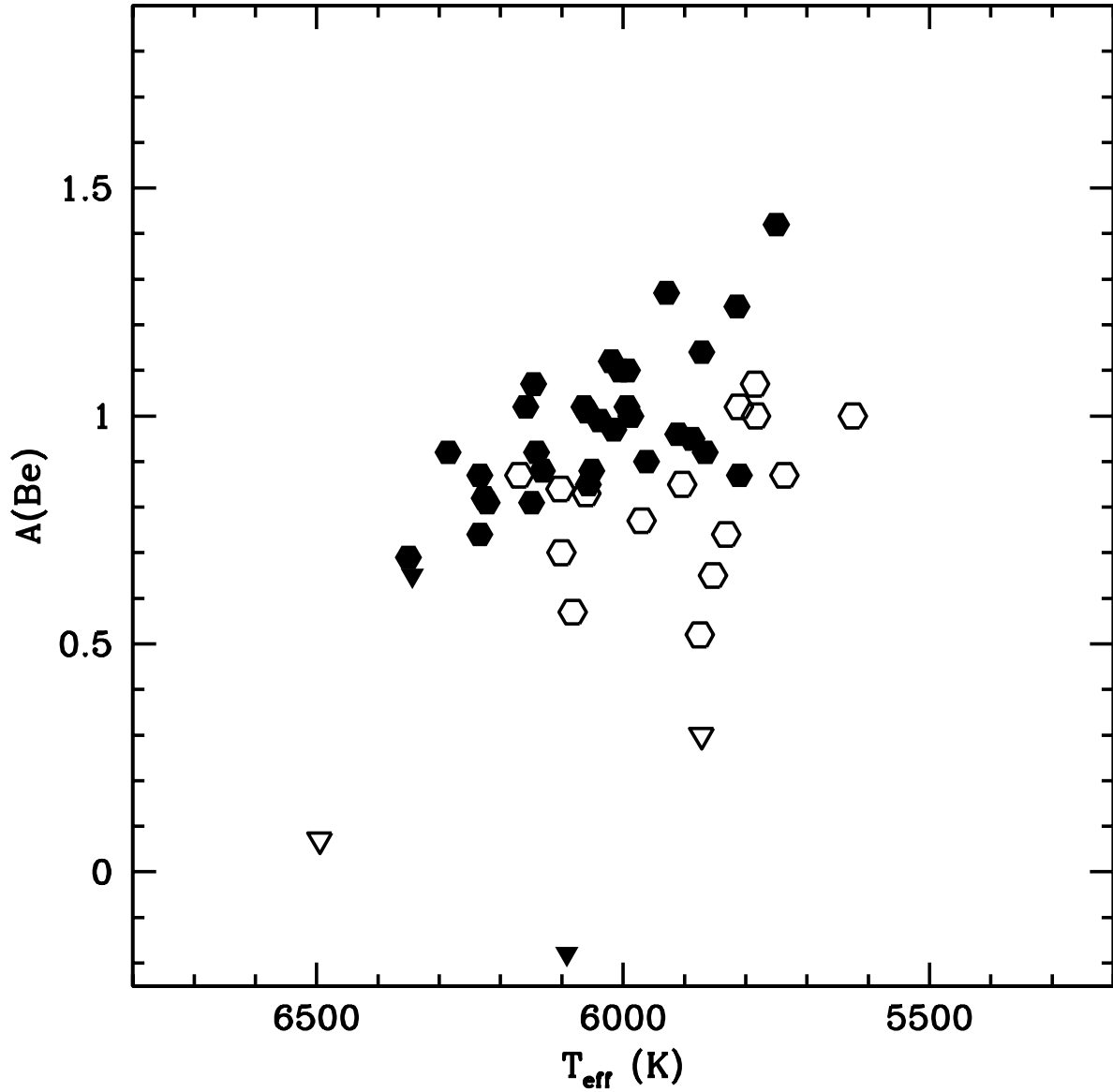


Fig. 9.— Distribution of $A(\text{Be})$ with T_{eff} . An upper envelope seems to be present showing an increase in $A(\text{Be})$ with decreasing temperature. The dwarf stars $-\log g > 4.1$ are filled symbols while the subgiants are open symbols. The triangles are upper limits. The subgiants show greater depletion of Be at a given temperature. This could indicate light element dilution caused by the expansion of convection zone.

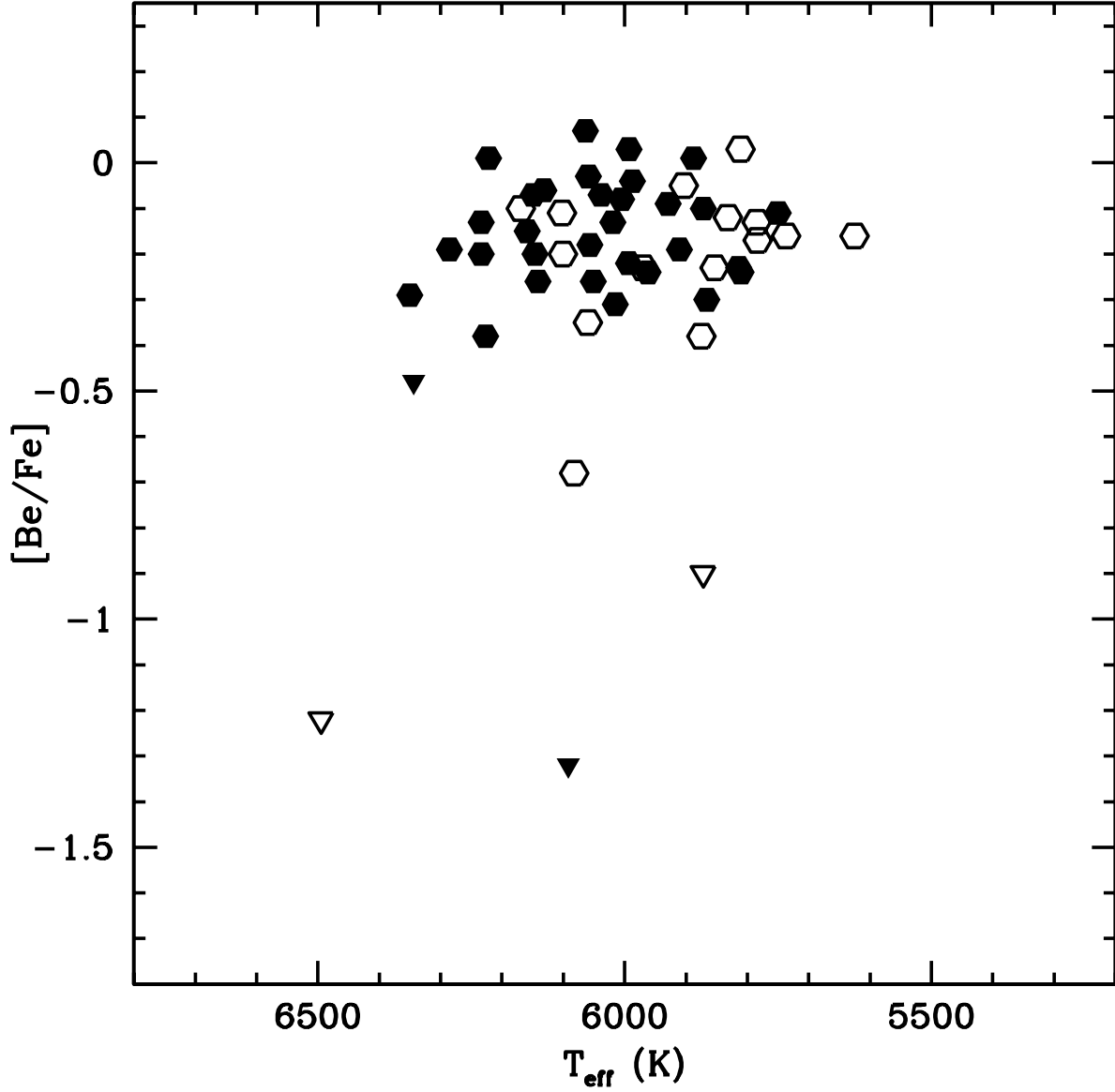


Fig. 10.— Distribution of $[Be/Fe]$ with T_{eff} . The dwarfs are filled symbols and the subgiants are open symbols. The upper envelope for detection is not present when the Be abundance is normalized to the Fe abundance. The values of $[Be/Fe]$ for dwarfs and subgiants appear to be similar.

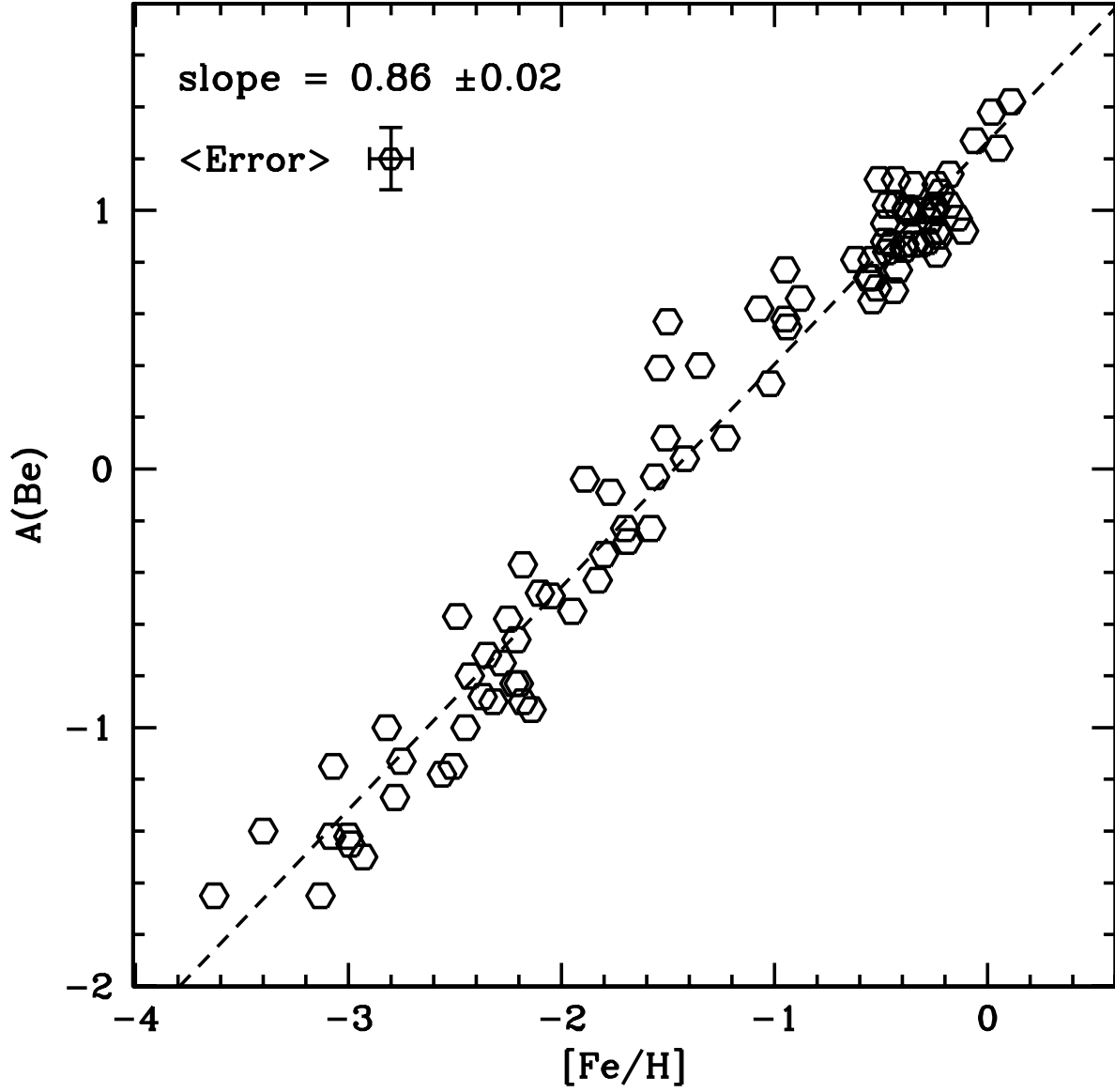


Fig. 11.— Be abundances from this study along with Boesgaard et al. (2008). As $[\text{Fe}/\text{H}]$ increases, $A(\text{Be})$ increases with a slope of 0.86 ± 0.02 , shown as the dashed line.

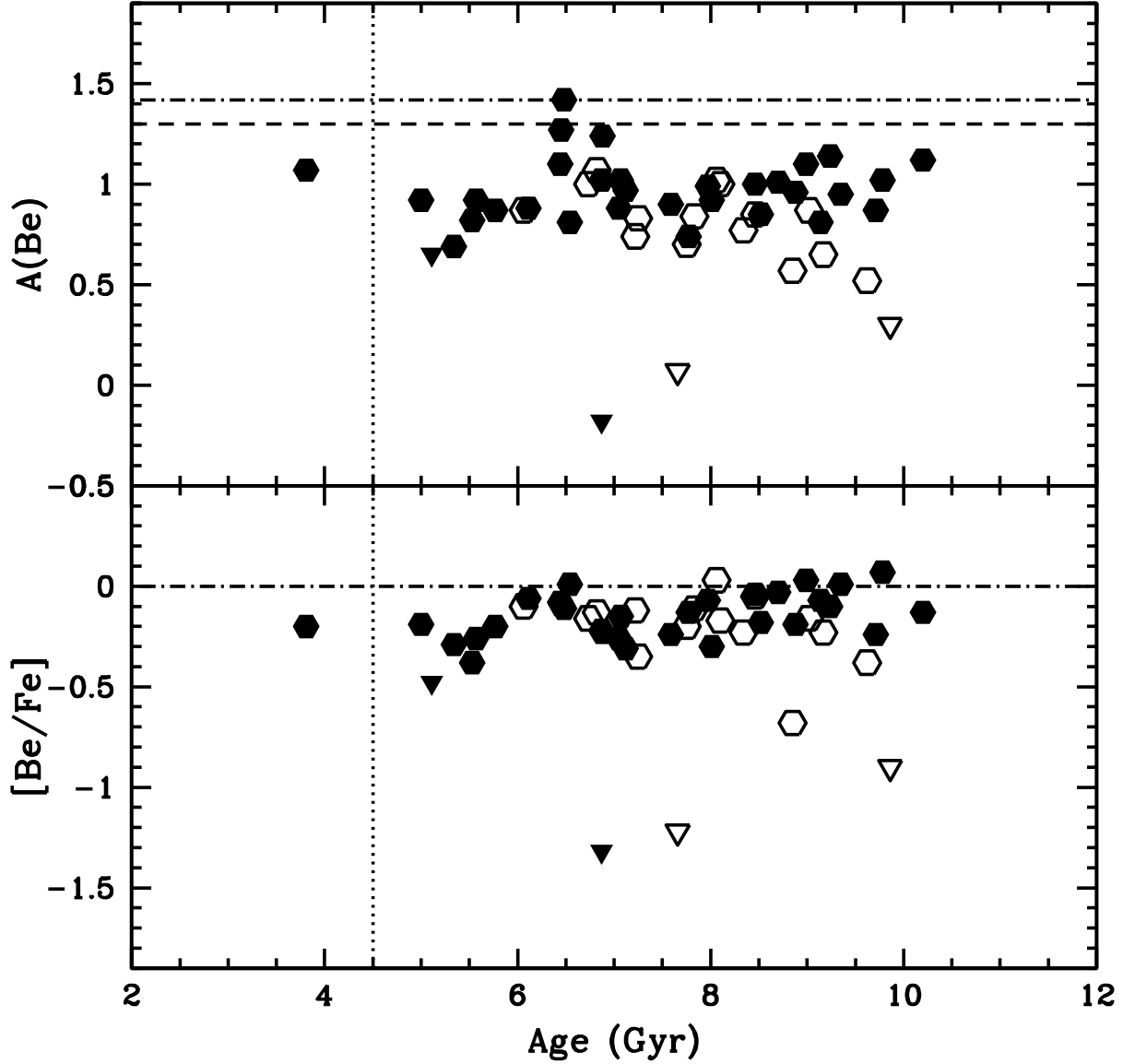


Fig. 12.— Be plotted as a function of age. The upper panel shows $A(\text{Be})$ while the lower panel has the Be abundance normalized to Fe and to the solar values. The meteoritic Be abundance, $A(\text{Be}) = 1.42$ is used for the solar system value. The filled hexagons are the dwarf stars and the open hexagons are subgiants as defined by $\log g < 4.1$. The triangles are Be upper limits. The vertical dotted line represents the age of the Sun. Only one star is younger than the Sun. In the upper panel the dashed line is placed at the approximate value of the solar Be abundance (Boesgaard 2003) and the dashed-dotted line represents the meteoritic Be abundance. As mentioned in the text, most of the LR04 stars are somewhat evolved off the zero age main-sequence and of the 157 stars in the mass range 0.9 to $1.1 M_{\odot}$ only 6 (or 4%) are < 5 Gyr in age. Given that these stars are older than the sun and have lower Be abundances, there is evidence for slow mixing during the main sequence stage of these stars.

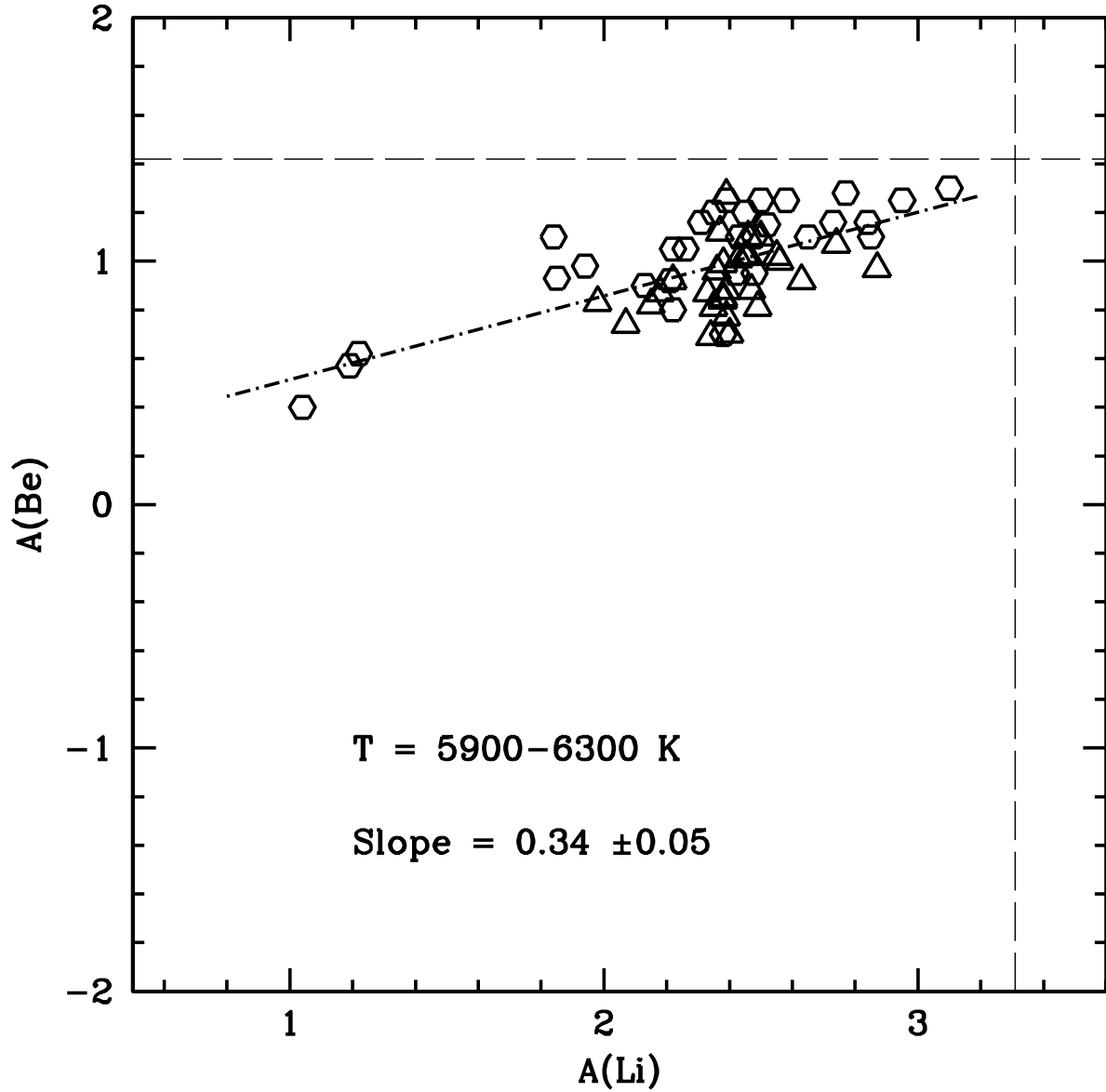


Fig. 13.— $A(\text{Be})$ plotted against $A(\text{Li})$ with the B01 and B04ab data. The triangles represent the stars from this study in the T_{eff} range 5900-6300 K; the hexagons represent the sample from B01 and B04ab. The one solar-mass stars fit the relationship well. The slope for all these stars is $+0.34 \pm 0.05$ which is consistent with the slope of 0.36 ± 0.05 given in B04a.

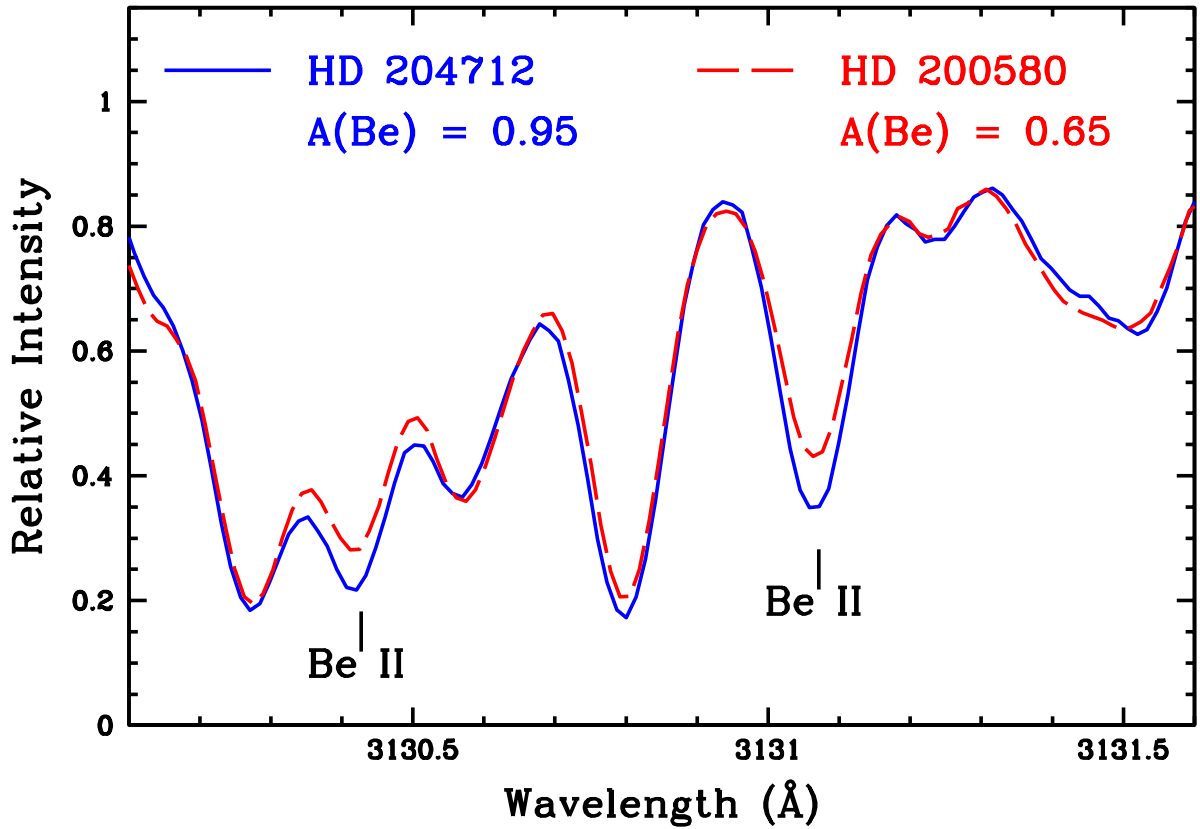


Fig. 14.— The Be region of the observed spectra of HD 204712 and HD 200580. The only difference in the two spectra is the strength of the two Be II features. The spectrum synthesis showed that these stars differ in their Be abundances by a factor of 2. They also differ in Li abundance by a factor of two, with HD 204712 having both more Be and more Li. The parameters of the two stars are virtually identical with 204712/200580 having $T_{\text{eff}} = 5888/5753$; $\log g = 4.05/4.12$; $[\text{Fe}/\text{H}] = -0.48/-0.54$; $\text{mass} = 0.96/0.95 M_{\odot}$; $\text{age} = 9.35/9.17$ Gyr.